AD-A065 627 MASSACHUSETTS INST OF TECH LEXINGTON LINCOLN LAB F/G 17/9
TARGET DETECTION WITH A DIRECT-RECEPTION OPTICAL RADAR.(U)
NOV 78 J H SHAPIRO F19628-78-C-0002.
UNCLASSIFIED TST-27 ESD-TR-78-290 NL

| OF |
AD
A065827

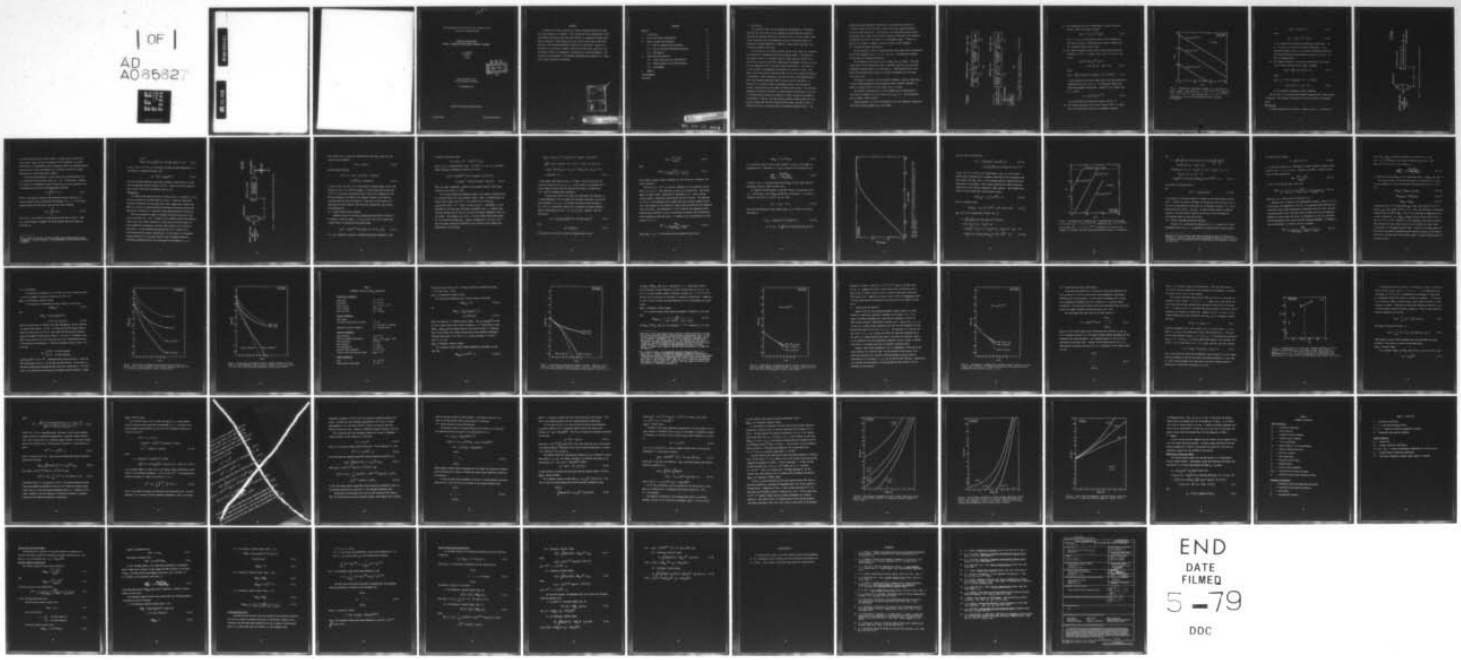

END
DATE
FILMED
5-79
DDC

MASSACHUSETTS INSTITUTE OF TECHNOLOGY
LINCOLN LABORATORY

# TARGET DETECTION WITH A DIRECT-RECEPTION OPTICAL RADAR

*J. H. SHAPIRO*
*Consultant*
*Group 53*



PROJECT REPORT TST-27
(Tactical Systems and Technology)

16 NOVEMBER 1978



LEXINGTON MASSACHUSETTS

## ABSTRACT

A theoretical study of the use of a direct reception Nd:YAG laser radar for target detection is reported. This work builds from a mathematical system model which incorporates the statistical effects of propagation through atmospheric turbulence, target speckle and glint, and receiver noise; both photomultiplier and avalanche photodiode receivers are considered. Results are presented for the receiver signal-to-noise ratio which show, explicitly, the deleterious effects of atmospheric scintillation on system performance. The structure and performance of the optimum likelihood-ratio processor for single-pulse target detection are analyzed.

CONTENTS

## I. Introduction

In a previous report [1] we examined the performance of a heterodyne-reception $CO_2$ laser radar in both imaging and target detection scenarios. The analysis contained therein was carried out only for clear-weather propagation conditions, but did incorporate realistic statistical models for propagation through atmospheric turbulence, target speckle and glint, and heterodyne-reception shot noise.

As discussed in [2], direct-reception Nd:YAG laser radars are candidates for pulsed-laser ranging and projectile-tracking systems. The purpose of the present report is to develop a body of target detection results for a Nd:YAG laser system to facilitate quantitative performance evaluation in general and comparison with a $CO_2$ laser system in particular. In Section II, we shall present a mathematical system model for the Nd:YAG radar. This model, which draws heavily upon the results of [1], will include the effects of turbulence, target interaction, and receiver noise; both photomultiplier (PMT) and avalanche photodiode (APD) receivers will be considered. In Section III, we shall use this system model to derive the single-pulse receiver signal-to-noise ratio (SNR) for PMT and APD systems. This material, although not directly indicative of target-detection performance, will allow us to quantitatively examine the effects of target speckle and atmospheric scintillation. Moreover, the SNR analysis provides simple quantitative comparisons between PMT and APD reception Nd:YAG radars, and may be used to compare Nd:YAG direct reception and $CO_2$ heterodyne reception radars. The

single-pulse target detection problem will be considered in Section IV. It turns out that the PMT and APD receivers both yield simple likelihood-ratio test (LRT) processors. Unfortunately, the associated receiver operating characteristic (ROC) results require numerical evaluation; this evaluation is underway, and will be the subject of a subsequent report. Finally, in Section V, we present a summary of the key results we have obtained.

## II. Nd:YAG Laser Radar Configuration

For our purposes, a direct-reception Nd:YAG laser radar may be represented by the block diagram of Fig. 1 (cf. [1, Fig. 3]). In drawing this diagram, we have made the following assumptions.

The transmitter and receiver will be taken to be co-located. The transmitter laser will be assumed to produce a periodic train of $t_p$-sec duration *rectangular-envelope pulses with peak power* $P_T$. These pulses will be transmitted from an unobscured circular exit pupil of diameter $d_T$ in the range $1 \text{ mm} \leq d_T \leq 5 \text{ mm}$.

The target of interest will be located a distance L from the radar along a line-of-sight propagation path through the clear turbulent atmosphere; L-values of interest will lie in the range $1 \text{ km} \leq L \leq 10 \text{ km}$.

The receiver entrance optics will be assumed to be an unobscured circular pupil of diameter $d_R$ in the range $10 \text{ cm} \leq d_R \leq 1 \text{ m}$. The photodetector will be either a *PMT* or an *APD*.

Making extensive use of the development in [1], the foregoing assumptions yield the following mathematical system model.

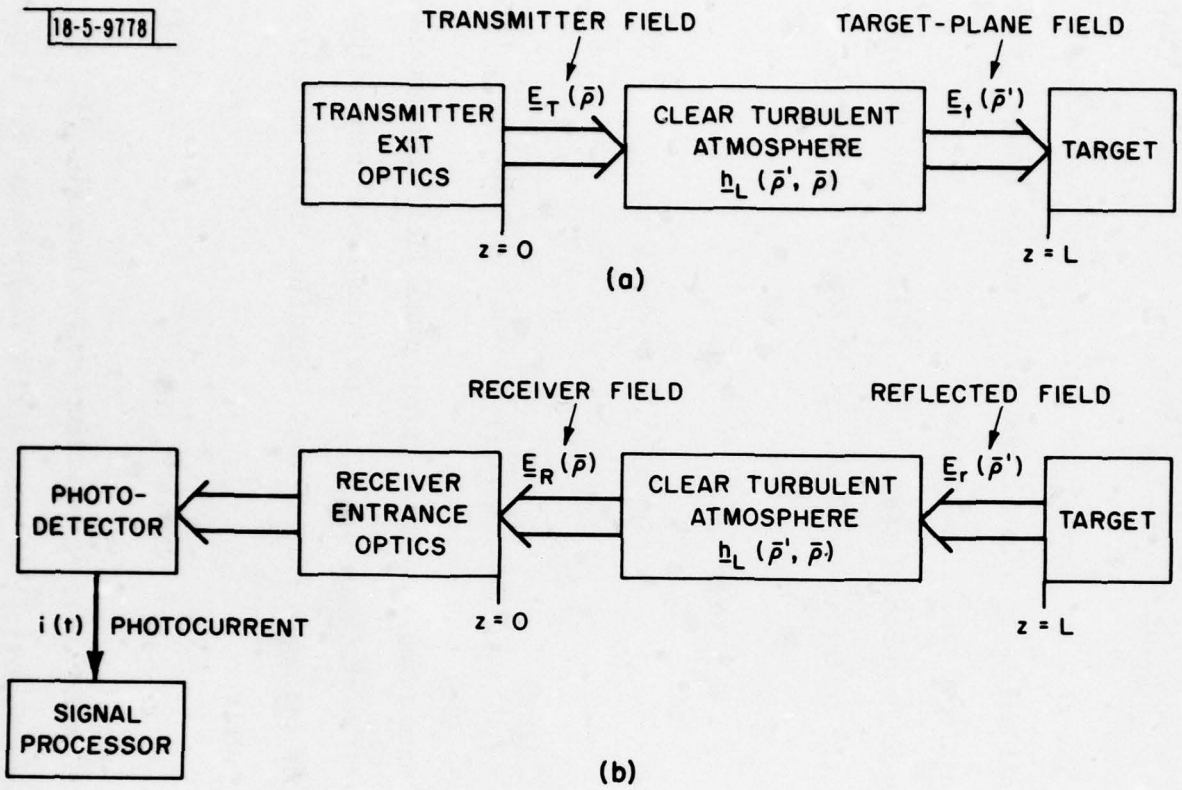


Fig.1. Nd:YAG laser radar configuration: (a) transmitter-to-target path, (b) target-to-receiver path.

(1) The transmitted wave has a monochromatic linearly polarized electric field with complex envelope

$$\underline{E}_T(\bar{\rho}) = (2P_T/c\varepsilon_o)^{1/2}\, \underline{\xi}_T(\bar{\rho}), \qquad \text{(II.1)}$$

for $\bar{\rho} = (x, y)$ a two dimensional vector in the transmitter's exit pupil and $\underline{\xi}_T(\bar{\rho})$ a normalized (unity square integral over the transmitter pupil) spatial mode.

(2) The complex envelope of the electric field arriving from the transmitter in the $z = L$ plane, $\underline{E}_t(\bar{\rho}')$ for $\bar{\rho}' = (x', y')$, satisfies

$$\underline{E}_t(\bar{\rho}') \approx (2P_T/c\varepsilon_o)^{1/2}\, \underline{\xi}_t(\bar{\rho}') \times \exp\,(\chi(\bar{\rho}', \bar{0}) + j\phi(\bar{\rho}', \bar{0})), \qquad \text{(II.2)}$$

where

$$\underline{\xi}_t(\bar{\rho}') \equiv \int d\bar{\rho}\; \underline{\xi}_T(\bar{\rho})(j\lambda L)^{-1} \exp[jkL(1 + |\bar{\rho}' - \bar{\rho}|^2/2L^2)] \qquad \text{(II.3)}$$

is the normalized free-space target plane field mode generated by transmission of $\underline{\xi}_T(\bar{\rho})$, and $\chi$, $\phi$ are turbulence-induced log-amplitude and phase fluctuations. Equation (II.2) assumes that $d_T < \rho_o$ where

$$\rho_o = (1.09\, k^2 C_n^2 L)^{-3/5} \qquad \text{(II.4)}$$

is the turbulence field coherence length (see Fig. 2).

(3) The complex envelope of the electric field in the $z = L$ plane that is directed back towards the transmitter satisfies

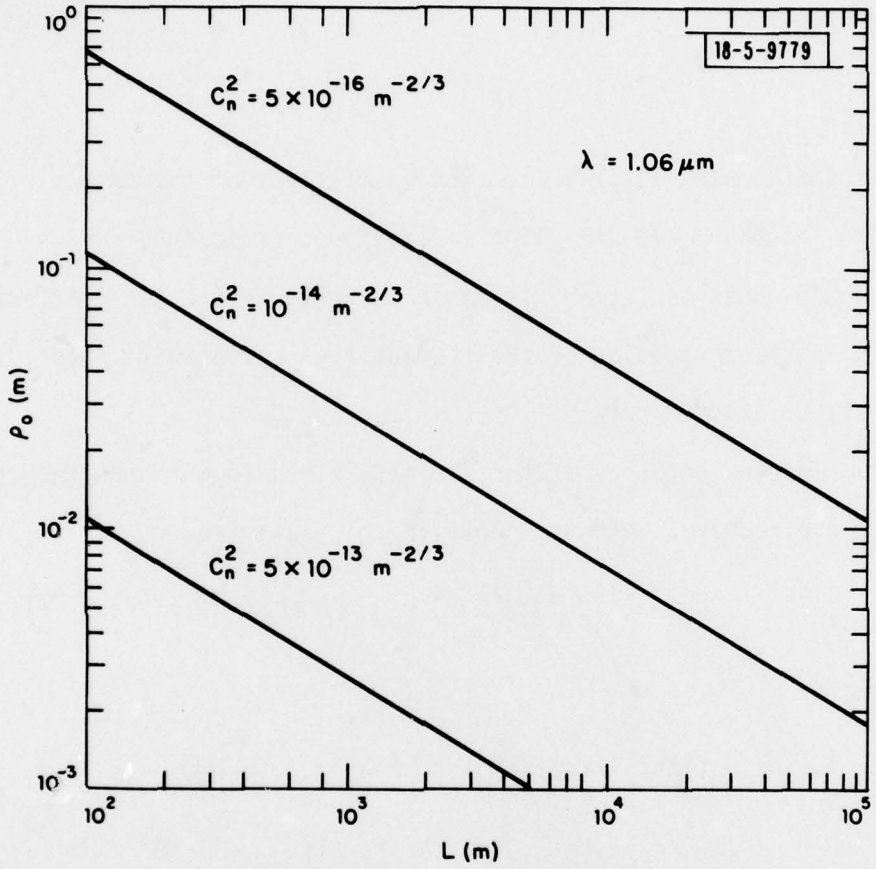


Fig.2. Turbulence coherence length $\rho_o$ vs propagation path length L for weak ($C_n^2 = 5 \times 10^{-16}\ m^{-2/3}$), moderate ($C_n^2 = 10^{-14}\ m^{-2/3}$), and strong ($C_n^2 = 5 \times 10^{-13}\ m^{-2/3}$) turbulence; 1.06 μm wavelength has been assumed throughout.

$$\underline{E}_r(\bar{\rho}') = \underline{E}_t(\bar{\rho}')\,\underline{T}(\bar{\rho}'), \tag{II.5}$$

where

$$\underline{T}(\bar{\rho}') = \underline{T}_g(\bar{\rho}')\, e^{j\theta} + \underline{T}_s(\bar{\rho}') \tag{II.6}$$

is the complex-field reflection coefficient of the target. In Eq. (II.6), $\underline{T}_g$ is the glint reflection coefficient, $\theta$ is a random phase angle, and $\underline{T}_s$ is the speckle reflection coefficient. The characterization of these quantities given in [1, Sect. III] will be assumed herein.

(4) The complex envelope of the electric field (due to the target) in the receiver entrance pupil, $\underline{E}_R(\bar{\rho})$, satisfies

$$\underline{E}_R(\bar{\rho}) = \int d\bar{\rho}'\, \underline{E}_r(\bar{\rho}')\, \underline{h}_L(\bar{\rho}', \bar{\rho}), \tag{II.7}$$

where

$$\underline{h}_L(\bar{\rho}', \bar{\rho}) = (j\lambda L)^{-1} \exp[jkL(1 + |\bar{\rho}' - \bar{\rho}|^2/2L^2)]$$

$$\times \exp[\chi(\bar{\rho}', \bar{\rho}) + j\phi(\bar{\rho}', \bar{\rho})] \tag{II.8}$$

is the stochastic atmospheric Green's function.

The statistics of the photocurrent depend on whether PMT or APD reception is employed. The relevant noise models for these receivers are developed below.

PMT Receiver

An idealized PMT optical receiver is shown in Fig. 3. It consists of

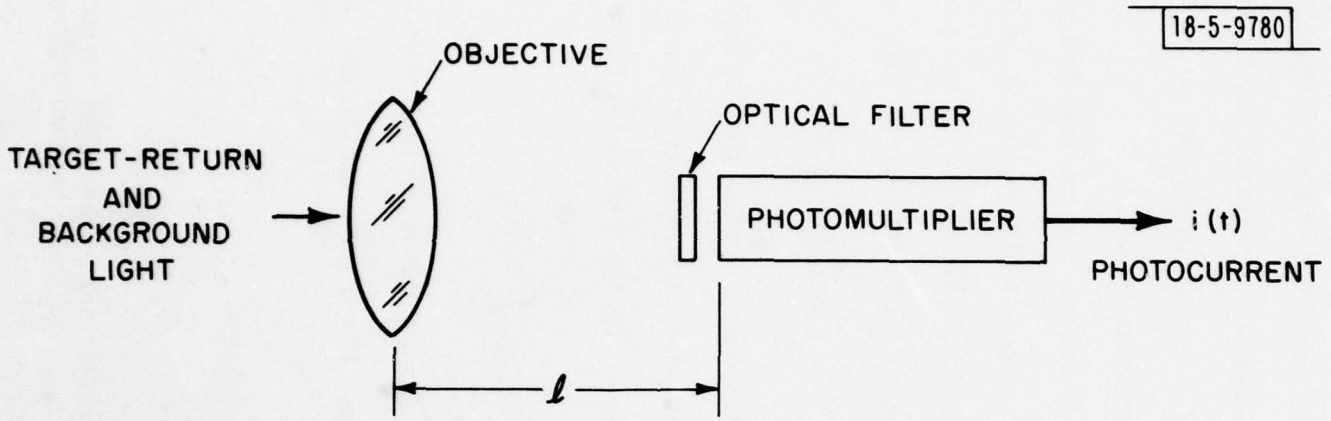


Fig.3. Photomultiplier receiver configuration.

a circular objective lens* (focal length $\ell$, diameter $d_R$) to collect and focus signal light, an optical-frequency filter (bandwidth $\Delta\lambda$ in wavelength units) to discriminate against background light, and a photomultiplier (circular active region of diameter $d_D$) to produce an electrical signal proportional to the incident optical power.

For typical PMT parameters, we may assume that the photocurrent $i(t)$ is a conditional Poisson point process [3] - [5]. In particular, assuming the receiver is illuminated by $\underline{E}_R(\bar{\rho})$ during the $t_p$-sec pulse duration, plus a broadband spatially-distributed background field then

$$N = \int_0^{t_p} d\tau\, q^{-1}\, i(\tau), \tag{II.9}$$

which is the number of photons counted during the pulse duration, is a Poisson random variable conditioned on knowledge of $\underline{T}$, $\chi$, $\phi$. This Poisson random variable has mean value (over the shot-noise ensemble)

$$\langle N \rangle_n = \int_0^{t_p} d\tau\, \mu(\tau), \tag{II.10}$$

where $\mu(t)$ is the effective average photon arrival rate at time t. When $d_D$ is large enough to encompass the entire angular spectrum of $\underline{E}_R(\bar{\rho})$ we find that [6]

---

*For $d_R$ values of interest, reflecting rather than refracting optics must be employed. The two, however, are interchangeable from a detection theory viewpoint.

$$\mu(t) \approx$$

$$(\eta/h\nu_o)\ [(c\varepsilon_o/2) \int d\bar{\rho}\ \text{circ}\ (2|\bar{\rho}|/d_R)\ |\underline{E}_R(\bar{\rho})|^2 + P_b] \qquad \text{(II.11)}$$

In Eqs. (II.9), (II.11), q is the charge released per photoabsorption, $\eta$ is the detector's quantum efficiency, and

$$P_b = \lambda^2 N_\lambda \Delta\lambda\ (\pi d_R d_D/4\lambda\ell)^2 \qquad \text{(II.12)}$$

gives the average background light power incident on the detector in terms of the background spectral radiance [7], [8]. (Note that we have neglected dark current, which would add another term to $\mu(t)$.)

APD Receiver

An idealized APD optical receiver is shown in Fig. 4. Basically, it has the same structure as the PMT receiver of Fig. 3. There are significant practical differences (a solid state APD is more rugged than a vacuum tube PMT, etc.) as well as marked analytical differences (basically Gaussian APD photocurrent statistics vs. basically Poisson PMT photocurrent statistics).

There are available a number of detailed statistical analyses of APD optical receivers [9] - [11]. We shall use the simple Gaussian approximation theory [12], [13], which is known [11] to give fairly accurate results in error probability calculations, and uses exact results for the signal-to-noise ratio. In this approach the photocurrent i(t) is taken to be a conditional Gaussian process. Specifically, if the receiver is illuminated by $\underline{E}_R(\bar{\rho})$ during the $t_p$-sec pulse interval, plus a broadband spatially-distributed background field, then conditioned on knowledge of $\underline{T}$, $\chi$, $\phi$,

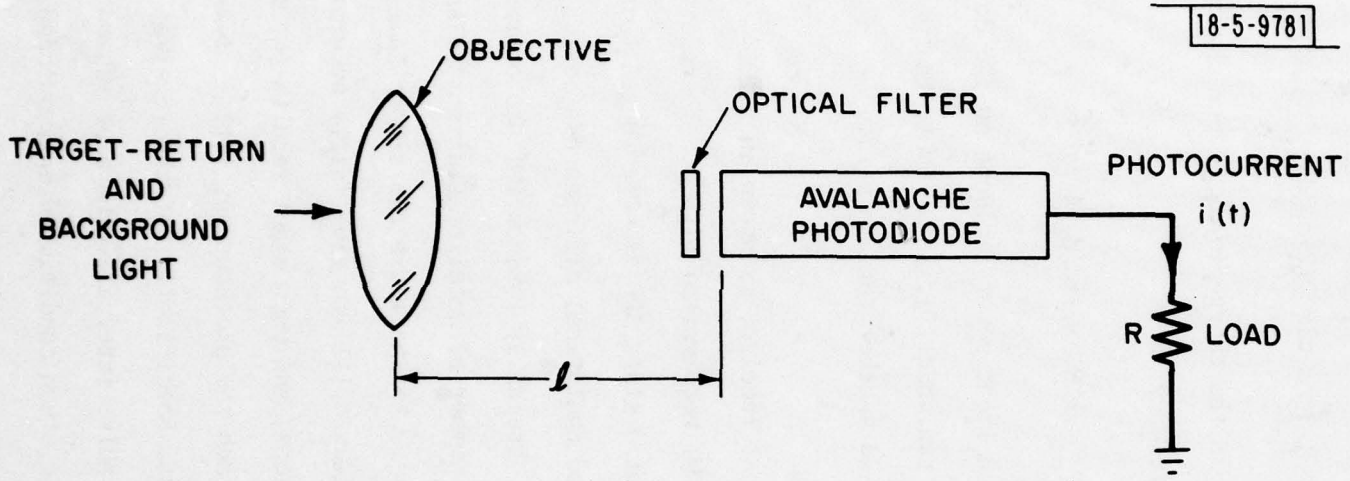


Fig.4. Avalanche photodiode receiver configuration.

the current i(t) is a Gaussian random process with mean value (over the receiver noise ensemble)

$$\langle i(t)\rangle_n = eG\mu(t) \tag{II.13}$$

and covariance function

$$\langle (i(t+\tau) - \langle i(t+\tau)\rangle_n)(i(t) - \langle i(t)\rangle_n)\rangle_n$$

$$= [e^2G^2F\,\mu(t) + 2kT/R]\,\delta(\tau). \tag{II.14}$$

in Eqs. (II.13), (II.14), $\mu(t)$ is the effective average photon arrival rate given by (II.11), e is electron charge, G is the average APD current gain, $F \approx G^{1/2}$ is the excess noise factor that is due to the randomness of the APD gain mechanism, and 2kT/R is the Johnson (thermal) noise spectrum associated with the load resistance R. (Note that in this model we are neglecting the noise figure of the electrical preamplifier that follows the photodetector.)

## III. Signal-To-Noise Ratio Analysis

Consider the use of the radar configuration described in Section II to observe a target at range L. As in [1, Sect. IV], let us assume that a single pulse is transmitted with spatial mode

$$\underline{\xi}_T(\bar{\rho}) = (4/\pi d_T^2)^{1/2} \exp\,(j2\pi \bar{f}_T \cdot \bar{\rho}),\ \text{for}\ |\bar{\rho}| \le d_T/2 \tag{III.1}$$

i.e., the transmitter radiates a collimated beam which propagates in the

direction of the unit vector

$$\bar{i}_T = [2\pi\bar{f}_T + (k^2 - |2\pi\bar{f}_T|^2)^{1/2}\ \bar{i}_z]/k$$

where $\bar{i}_z$ is a +z directed unit vector. For $d_T^2/\lambda L < 1$, $d_T < \rho_o$, the target-plane field $\underline{E}_t(\bar{\rho}')$ therefore satisfies (II.2) with

$$\underline{\xi}_t(\bar{\rho}') \approx (\pi d_T^2/4)^{1/2}\ (j\lambda L)^{-1}\ \exp(jkL + jk|\bar{\rho}'|^2/2L)$$

$$\times\ J_1(\pi d_T|\bar{\rho}' - \lambda L\bar{f}_T|/\lambda L)/(\pi d_T|\bar{\rho}' - \lambda L\bar{f}_T|/2\lambda L). \quad \text{(III.2)}$$

Thus, the radar illuminates a nominal $\lambda L/d_T$ diameter region of the target centered on the point $\bar{\rho}' = \lambda L\bar{f}_T$.

For realistic projectile-tracking scenarios, the target of interest will lie entirely within this $\lambda L/d_T$ diameter region. Hence, in computing $\underline{E}_R$, the target-return field, from (II.5) - (II.8) and (III.2) we may use $\underline{\xi}_t(\lambda L\bar{f}_T)\exp(j2\pi\bar{f}_T \cdot (\bar{\rho}' - \lambda L\bar{f}_T))$ in place of $\underline{\xi}_t(\bar{\rho}')$. Furthermore, it will typically be true that $d_R/L$ (the angle subtended in the z = L plane by the receiver entrance optics) will be less than the angular beamwidth of the target return. This enables us to use $\bar{\rho} = \bar{0}$ in the Fresnel diffraction kernel in (II.8) when we calculate $\underline{E}_R$. Finally, assuming (as in [1, Sect. IV]) that the target reflection coefficient may be treated in the single-glint approximation, we find that

$$\underline{E}_R(\bar{\rho}) \approx (2P_T/c\varepsilon_o)^{1/2}\, \underline{\xi}_t(\lambda L \bar{f}_T)(j\lambda L)^{-1} \exp(jkL - j4\pi\lambda L\,|\bar{f}_T|^2)$$

$$\times \int d\bar{\rho}'\, \{\underline{T}_s(\bar{\rho}') \exp[\chi(\bar{\rho}', \bar{0}) + \chi(\bar{\rho}', \bar{\rho}) + j(\phi(\bar{\rho}', \bar{0}) + \phi(\bar{\rho}', \bar{\rho}))]$$

$$+ \underline{T}_g(\bar{\rho}') \exp[\chi(\bar{\rho}'_g, \bar{0}) + \chi(\bar{\rho}'_g, \bar{\rho}) + j(\phi(\bar{\rho}'_g, \bar{0}) + \phi(\bar{\rho}'_g, \bar{\rho}) + \theta)]\}$$

$$\times \exp(j4\pi \bar{f}_T \cdot \bar{\rho}'), \qquad \text{(III.3)}$$

is the target-return field in the $z = 0$ plane. Using (III.3) with the statistics given in [1] for $\underline{T}_s$, $\chi$, $\phi$, $\theta$ will enable us to evaluate the receiver signal-to-noise ratio for PMT and APD systems, as shown below.

III.1 SNR for Photomultiplier Reception

It may be seen from (II.11) that the conditional rate function $\mu(t)$ is time-independent, for all target and turbulence conditions, during the pulse interval $0 \leq t \leq t_p$. As a result the interval count N given by Eq. (II.9) is a sufficient statistic for estimation of target parameters based on observation of $\{i(t) : 0 \leq t \leq t_p\}$ [14]. Moreover, with the definitions

$$n_s = (c\varepsilon_o \eta t_p/2h\nu_o) \int d\bar{\rho}\, \text{circ}\,(2|\bar{\rho}|/d_R)\ |\underline{E}_R(\bar{\rho})|^2, \qquad \text{(III.4)}$$

and

$$n_b = \eta P_b t_p/h\nu_o, \qquad \text{(III.5)}$$

the analysis of [6] tells us that the signal-to-noise ratio

$$\mathrm{SNR} \equiv \frac{(\langle N \rangle - n_b)^2}{\mathrm{Var}(N)} \tag{III.6}$$

obeys

$$\mathrm{SNR} = \frac{\langle n_s \rangle}{1 + \mathrm{Var}(n_s)/\langle n_s \rangle + n_b/\langle n_s \rangle} \tag{III.7}$$

where angular brackets denote averaging over the shot-noise, turbulence, and target ensembles.

Physically Eq. (III.7) is directly analogous to the heterodyne-receiver SNR [1, Eq. (IV.7)]. The quantities $n_s$ and $n_b$ are, respectively, the average number of signal counts (conditioned on knowledge of $\underline{T}$, $\chi$, and $\phi$) and the average number of background counts during the pulse interval. The numerator in (III.7) is the quantum-limited (signal shot-noise limited) signal-to-noise ratio that prevails in the absence of target-return fluctuations and background-light shot noise. The denominator in (III.7) measures the degradation from quantum-limited SNR that is due to the presence of target-return fluctuations and/or background-light shot noise. To emphasize this interpretation we shall rewrite (III.7) as

$$\mathrm{SNR} = \frac{\mathrm{SNR}_q}{1 + \mathrm{SNR}_q/\mathrm{SNR}_{\mathrm{SAT}} + (\mathrm{SBR})^{-1}}, \tag{III.8}$$

where $\mathrm{SNR}_q \equiv \langle n_s \rangle$ is the quantum-limited signal-to-noise ratio,

$$SNR_{SAT} \equiv \langle n_s \rangle^2 / Var(n_s) \qquad (III.9)$$

is a saturation signal-to-noise ratio, and $SBR \equiv \langle n_s \rangle / n_b$ is the signal-to-background ratio. When $SBR \geq 10$, (III.8) reduces to the universal curve

$$\frac{SNR}{SNR_{SAT}} = \frac{SNR_q / SNR_{SAT}}{1 + SNR_q / SNR_{SAT}} ; \qquad (III.10)$$

as shown in Fig. 5, increasing $SNR_q$ beyond $SNR_{SAT}$ in this regime does not appreciably increase signal-to-noise ratio.

To complete the SNR analysis of the PMT receiver, we need only find $\langle n_s \rangle$ and $Var(n_s)$ so that $SNR_{SAT}$ and SBR may be evaluated. It is easy to calculate, from (III.3), (III.4) and [1], that

$$\langle n_s \rangle = \langle n_s \rangle_g + \langle n_s \rangle_s \qquad (III.11)$$

gives the unconditioned average signal count $\langle n_s \rangle$ in terms of its glint contribution

$$\langle n_s \rangle_g = (\eta P_T t_p / h\nu_o L^2) \; |\underline{\xi}_t(\lambda L \bar{f}_T)|^2 A_T \qquad (III.12)$$

$$x \, \rho'(\lambda; \bar{f}_T; -\bar{f}_T) \int d\bar{\rho} \, \mathrm{circ}(2|\bar{\rho}|/d_R) \exp(4C_{XX}(\bar{0}, \bar{\rho})),$$

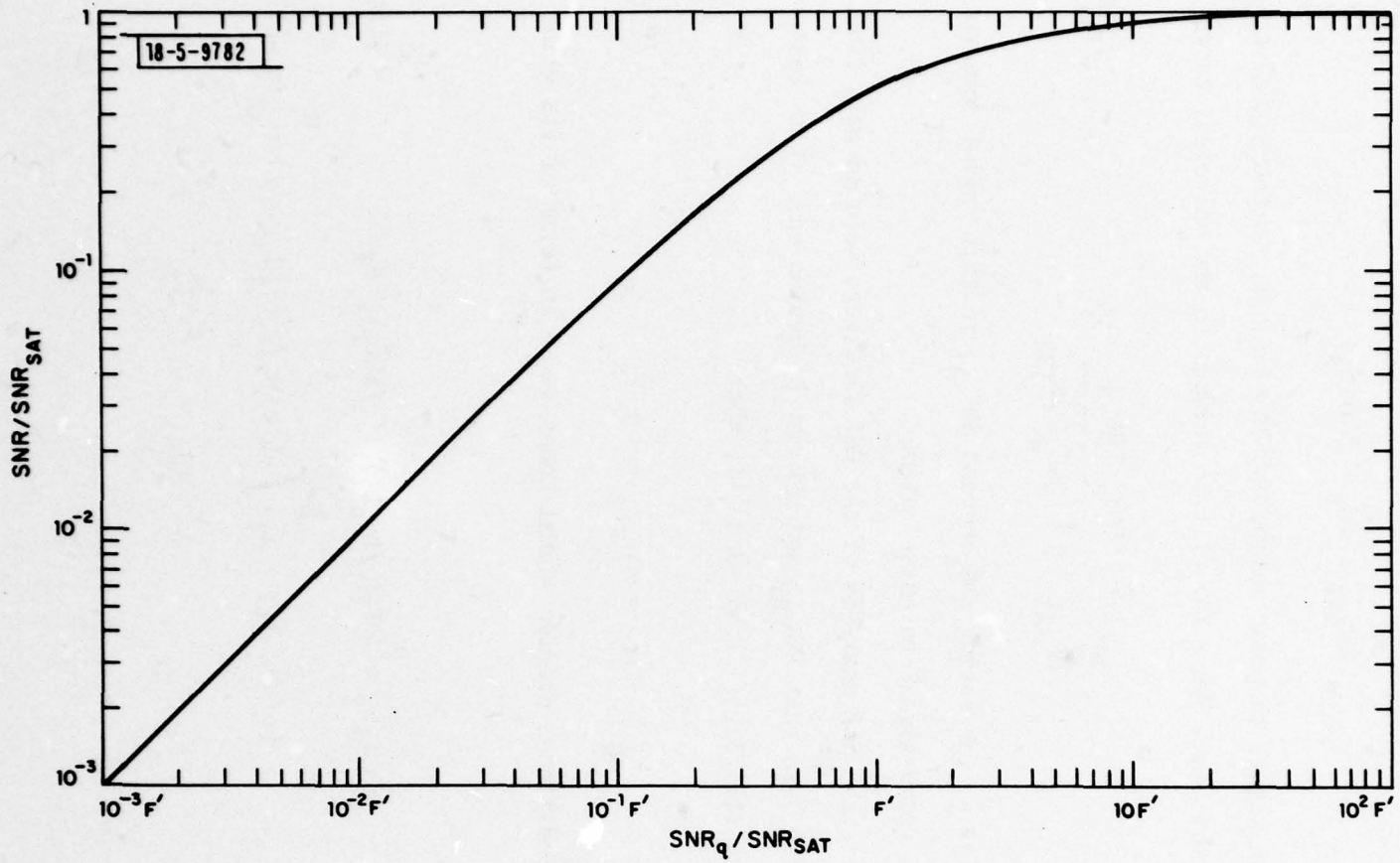


Fig.5. Universal curves for normalized receiver signal-to-noise ratio for PMT reception (F' = 1, see Eq.(III.10)) and APD reception (F' = F, see Eq.(III.23)).

and its speckle contribution

$$\langle n_s \rangle_s = (\eta P_T t_p / h\nu_o L^2) \; |\underline{\xi}_t(\lambda L \bar{f}_T)|^2 A_T \qquad \text{(III.13)}$$

$$\times \; T_s(\lambda L \bar{f}_T) \int d\bar{\rho} \; \text{circ}\,(2|\bar{\rho}|/d_R) \exp\,(4C_{\chi\chi}(\bar{0}, \bar{\rho}))$$

In Eqs. (III.12), (III.13), $A_T$ is the target's area, $\rho'$ is the target's bidirectional reflectance for a specular reflection of the illuminator beam back towards the radar, and $T_s$ is the average intensity diffuse-reflection coefficient of the target. Both of these equations are merely notational translations of the familiar monostatic radar equation. With somewhat more effort it can be shown that for a pure-glint target

$$\text{Var}(n_s)_g = \langle n_s \rangle_g^2 \, \zeta' (e^{16\sigma_\chi^2} - 1), \qquad \text{(III.14)}$$

and for a speckle target

$$\text{Var}(n_s)_s = \langle n_s \rangle_s^2 \, [\zeta'' (e^{16\sigma_\chi^2} - 1) \, (\mathcal{D}^o + 1)/\mathcal{D}^o + 1/\mathcal{D}^o] \qquad \text{(III.15)}$$

where $\sigma_\chi^2$ is the log-amplitude variance (Fig. 6),

$$\zeta' = [\int d\bar{\rho}_1 \int d\bar{\rho}_2 \; \text{circ}\,(2|\bar{\rho}_1|/d_R) \; \text{circ}\,(2|\bar{\rho}_2|/d_R)$$

$$\times \exp\,(4C_{\chi\chi}(\bar{0}, \bar{\rho}_1) + 4C_{\chi\chi}(\bar{0}, \bar{\rho}_2))$$

$$\times \, (\exp(4\sigma_\chi^2 + 4C_{\chi\chi}(\bar{0}, \bar{\rho}_1) + 4C_{\chi\chi}(\bar{0}, \bar{\rho}_2) + 4C_{\chi\chi}(\bar{0}, \bar{\rho}_1 - \bar{\rho}_2)) - 1)]$$

$$\div \, [(\int d\bar{\rho} \; \text{circ}\,(2|\bar{\rho}|/d_R) \exp\,(4C_{\chi\chi}(\bar{0}, \bar{\rho})))^2 \; (e^{16\sigma_\chi^2} - 1)] \qquad \text{(III.16)}$$

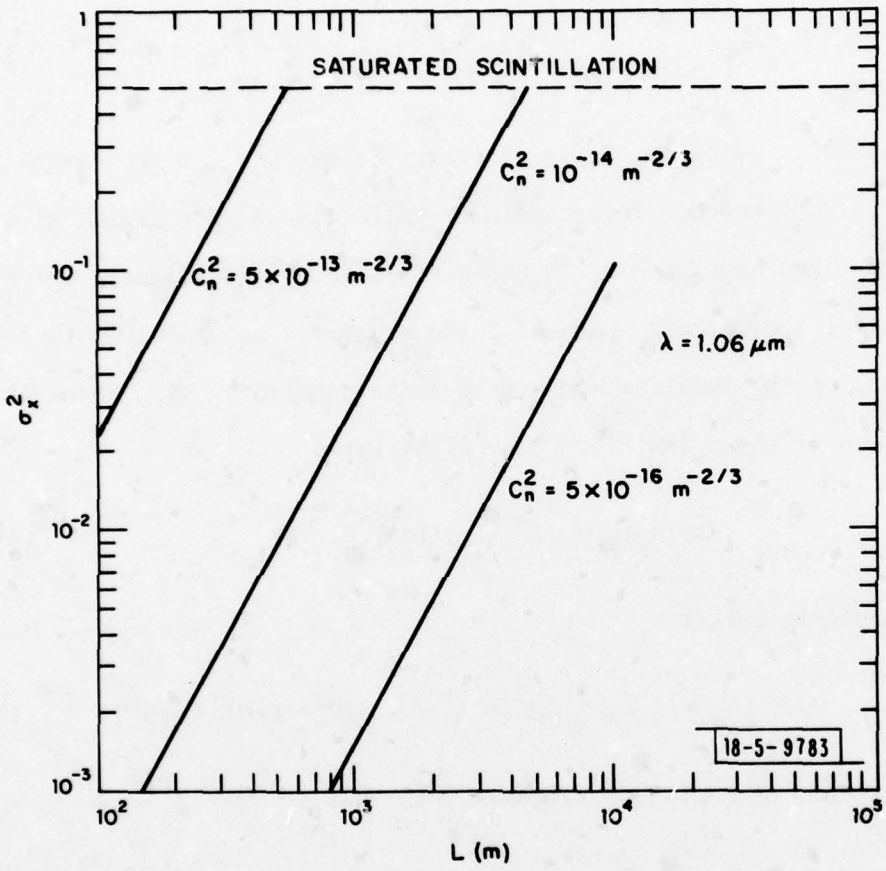


Fig.6. Log-amplitude variance $\sigma_\chi^2$ vs propagation path length L for weak ($C_n^2 = 5 \times 10^{-16}\ m^{-2/3}$), moderate ($C_n^2 = 10^{-14}\ m^{-2/3}$), and strong ($C_n^2 = 5 \times 10^{-13}\ m^{-2/3}$) turbulence; 1.06 μm wavelength is assumed and the weak perturbation theory is employed.

and

$$\zeta'' = \{\int d\bar{\rho}_1 \int d\bar{\rho}_2 \,\mathrm{circ}\,(2|\bar{\rho}_1|/d_R)\,\mathrm{circ}\,(2|\bar{\rho}_2|/d_R) \int_{A_T} d\bar{\rho}_1' \int_{A_T} d\bar{\rho}_2'$$
$$\times \exp(4C_{\chi\chi}(\bar{0}, \bar{\rho}_1) + 4C_{\chi\chi}(\bar{0}, \bar{\rho}_2))$$
$$\times[\exp(4C_{\chi\chi}(\bar{\rho}_1' - \bar{\rho}_2', \bar{0}) + 4C_{\chi\chi}(\bar{\rho}_1' - \bar{\rho}_2', \bar{\rho}_1) + 4C_{\chi\chi}(\bar{\rho}_1' - \bar{\rho}_2', -\bar{\rho}_2)$$
$$+ 4C_{\chi\chi}(\bar{\rho}_1' - \bar{\rho}_2', \bar{\rho}_1 - \bar{\rho}_2)) - 1]\}$$
$$\div [(A_T \int d\bar{\rho}\,\mathrm{circ}\,(2|\bar{\rho}|/d_R)\,\exp(4C_{\chi\chi}(\bar{0}, \bar{\rho})))^2 (e^{16\sigma_\chi^2} - 1)] \qquad \text{(III.17)}$$

are aperture-averaging factors,

and

$$v^o \approx 1 + \pi d_R^2 A_T/4(\lambda L)^2, \qquad \text{(III.18)}$$

is the number of free-space degrees of freedom in the diffuse-target observation*. A result can also be obtained for the general form of $\mathrm{Var}(n_s)$, but it will not be presented here; when there is no turbulence, however, it is easily demonstrated that $\mathrm{Var}(n_s) = \mathrm{Var}(n_s)_s$. We shall consider specific numerical examples of the PMT receiver signal-to-noise ratio after we develop the corresponding theory for the APD receiver.

III.2 SNR for Avalanche Photodiode Reception

Because i(t), conditioned on knowledge of $\underline{T}$, $\chi$, $\phi$, consists of a time-independent mean for $0 \leq t \leq t_p$ embedded in an additive white Gaussian noise,

---

*Equation (III.17) is derived under some approximations that are discussed in Section IV. Moreover, some care must be exercised in using (III.16), (III.17), as saturation of scintillation will be encountered in the scenarios of interest (see Fig. 6).

the matched-filter output

$$N' \equiv \int d\tau \, (eG)^{-1} i(\tau) \tag{III.19}$$

is a sufficient statistic for estimation of target parameters based on observation of $\{i(t) : 0 \leq t \leq t_p\}$ [15]. Defining, therefore, a signal-to-noise ratio for APD reception by

$$SNR \equiv \frac{(<N'> - n_b)^2}{Var(N')} , \tag{III.20}$$

(II.13), (II.14) may be used to show that

$$SNR = \frac{<n_s>}{F(1 + n_b/<n_s>) + Var(n_s)/<n_s> + 2kTt_p/Re^2G^2<n_s>} , \tag{III.21}$$

where $n_b$, $<n_s>$, $Var(n_s)$ are as in Section III.1.

Equation (III.21) admits to an interpretation similar to that of (III.7). In particular, the numerator in (III.21) is the quantum-limited SNR that prevails when target-return fluctuations, background-light shot noise, APD gain-fluctuation excess noise, and load resistor thermal noise may be neglected compared to signal-light shot noise; the denominator in (III.21) quantifies the SNR degradations that result from the foregoing phenomena. To emphasize this interpretation, we rewrite (III.21) as follows

$$SNR = \frac{SNR_q}{F + SNR_q/SNR_{SAT} + F(SBR)^{-1} + (STR)^{-1}} , \tag{III.22}$$

where $SNR_q$, $SNR_{SAT}$, and SBR are defined as in Section III.1, and $STR \equiv \langle n_s \rangle e^2G^2R/2kTt_p$ is the signal-to-thermal noise ratio. When $SBR \geq 10$, $STR \geq 10/F$, (III.22) reduces to

$$\frac{SNR}{SNR_{SAT}} \approx \frac{SNR_q/SNR_{SAT}}{F + SNR_q/SNR_{SAT}} ; \qquad \text{(III.23)}$$

if follows that $SNR \approx SNR_{SAT}$ in this regime when $SNR_q \geq F\ SNR_{SAT}$ (see Fig. 5).

The relative merits of PMT and APD reception, as measured by a signal-to-noise comparison, can be qualitatively discerned from (III.8), (III.22) and

$$SNR_{qAPD} = SNR_{qPMT}\ \eta_{APD}/\eta_{PMT}, \qquad \text{(III.24)}$$

$$(SNR_{SAT})_{APD} = (SNR_{SAT})_{PMT}, \qquad \text{(III.25)}$$

$$SBR_{APD} = SBR_{PMT}. \qquad \text{(III.26)}$$

In particular, at 1.06 μm wavelength $\eta_{PMT}$ values range from $10^{-3}$ to $10^{-2}$, whereas $\eta_{APD}$ values range from 0.1 to 0.5. Thus, the APD enjoys a substantial advantage over the PMT in $SNR_q$. Part of this advantage is immediately lost to gain fluctuations, viz. $SNR_{APD} \leq SNR_q/F$ follows directly from (III.22), and $F \approx 10$ for $G = 100$. Moreover, at very high $SNR_q$ values both the PMT and APD receivers will have signal-to-noise ratios limited, by target-return fluctuations, to the same saturation value. Finally, at low $SNR_q$ values the PMT receiver may vastly outperform the APD receiver, because of the thermal noise that is present only in the latter system. Detailed examples appear in the next section.

III.3 SNR Examples

To illustrate the behavior of (III.8) and (III.22), we shall consider a series of examples analogous to those of [1, Sect. IV].

Case 1 No Turbulence, Specular Target

In the absence of turbulence and target speckle, we find that,

$$SNR^{o}_{gSAT} = \infty, \tag{III.27}$$

and

$$SNR^{o}_{gq} = \eta P_T t_p (\pi d_T d_R / 4\lambda L)^2 A_T \times \rho'(\lambda; \bar{f}_T; -\bar{f}_T)/h\nu_o L^2, \tag{III.28}$$

where the superscript "o" denotes free-space propagation, and the subscript "g" denotes glint target. In Fig. 7 we have plotted the quantum-limited signal-to-noise ratio (III.28) vs. path length for PMT and APD reception, using the parameter values given in Table 1. As in [1], we include in Fig. 7 $SNR^{o}_{q}$ curves given by (III.28) times $\exp(-2\alpha L)$, for a representative value of the extinction coefficient $\alpha$. Using the parameters given in Table 1, we find that

$$n_b = \begin{cases} 0.206, & \text{for PMT reception} \\ 10.3, & \text{for APD reception} \end{cases}$$

and $2kTt_p/Re^2G^2 = 3.23 \times 10^4$. Combining these results with Fig. 7 gives the SNR curves shown in Fig. 8. We see that the PMT receiver, in this case, is basically unaffected by background-light shot noise except when $\alpha = 0.41$ km$^{-1}$ and $L \geq 8$ km, whereas the APD receiver performance shows the effect of gain-

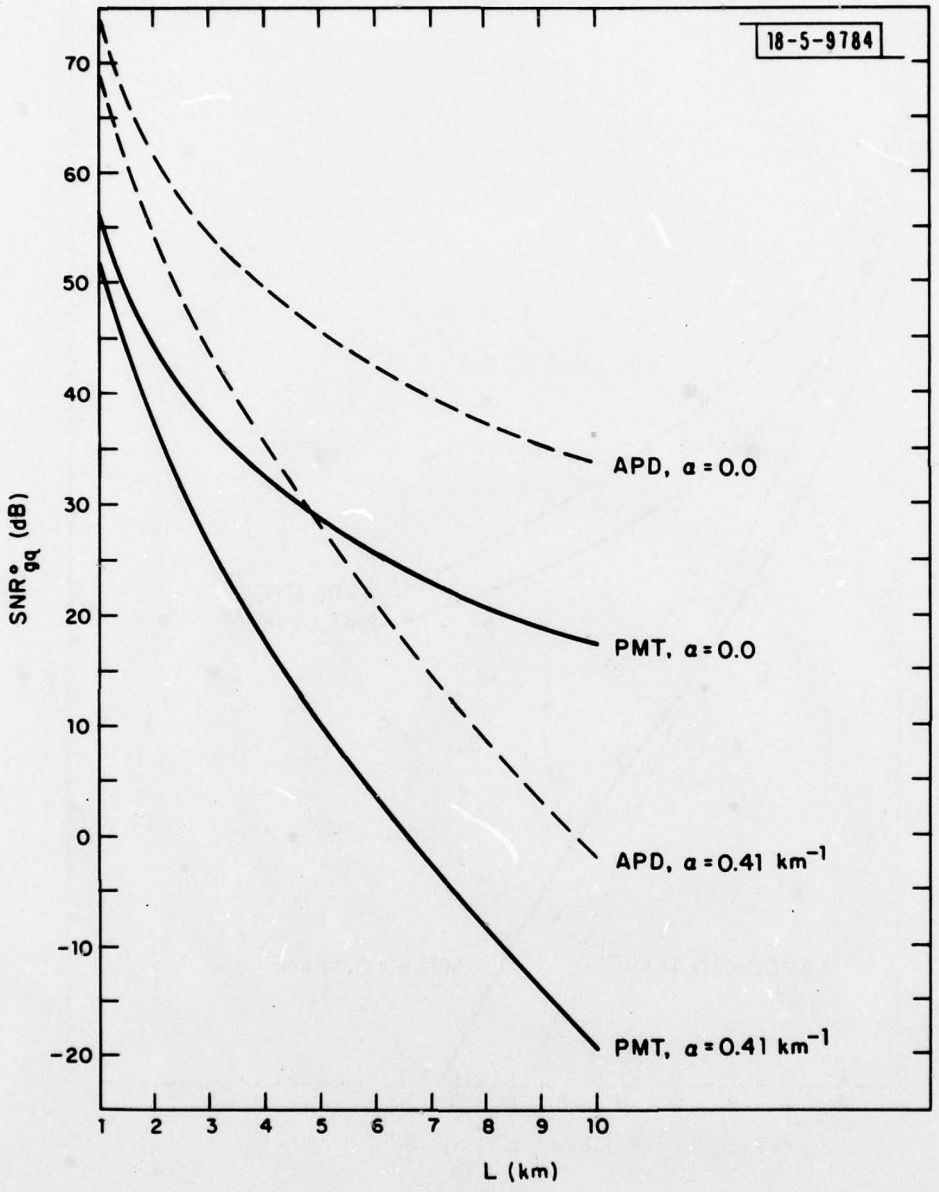


Fig.7. Free-space propagation quantum limited signal-to-noise ratio vs path length L for a glint target; Eq.(III.28) is used with the parameter values from Table 1.

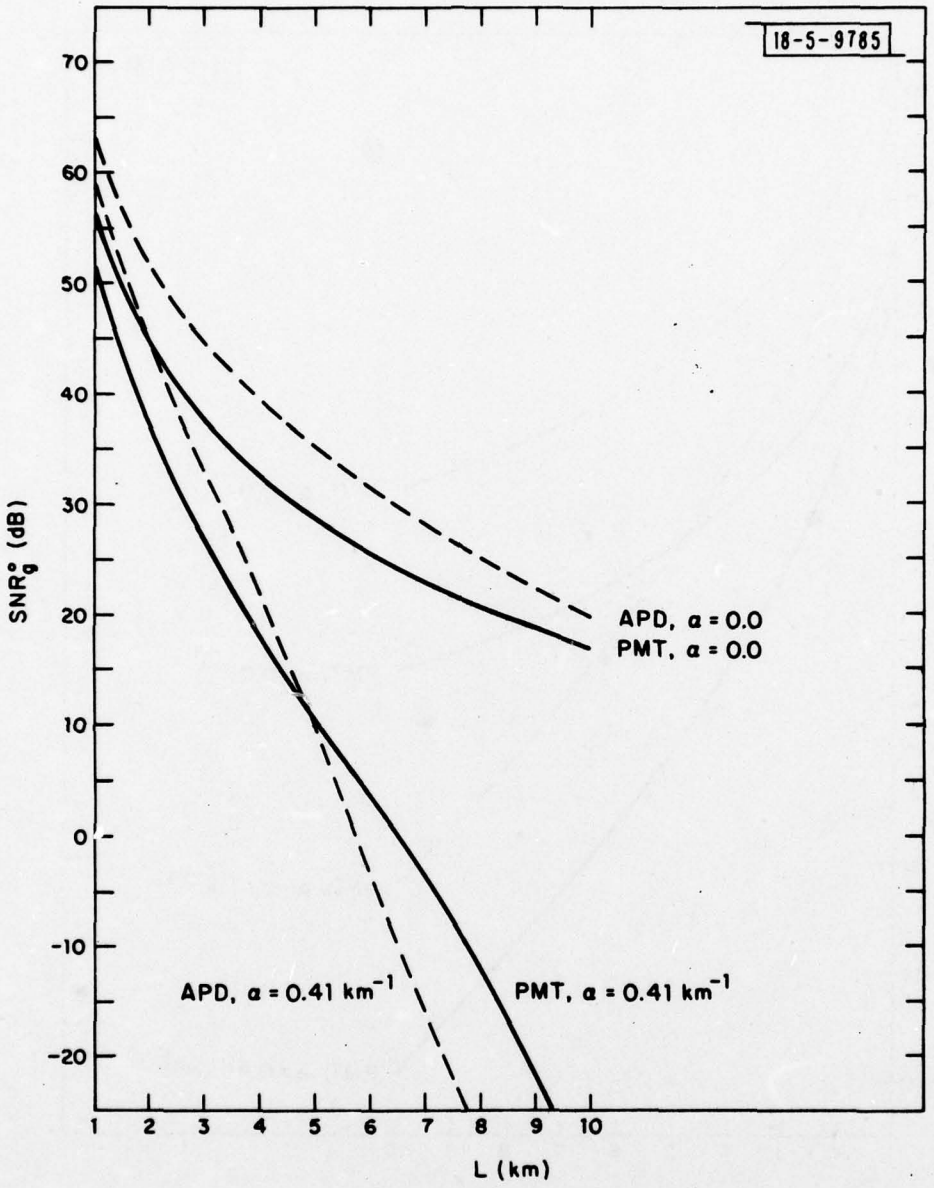


Fig.8. Free-space propagation glint target signal-to-noise ratio vs path length L; Eqs.(III.8), (III.22), (III.27), and (III.28) are used with the parameter values from Table 1.

TABLE I

PARAMETER VALUES FOR $SNR^{o}_{gq}$ EVALUATION

| | |
|---|---|
| **Transmitter Parameters** | |
| peak power | $P_T = 10^5$ W |
| wavelength | $\lambda = 1.06$ μm |
| photon energy | $h\nu_o = 1.87 \times 10^{-19}$ J |
| pupil diameter | $d_T = 5$ mm |
| pulse duration | $t_p = 50$ nsec |
| **Channel Parameters** | |
| path length | L |
| extinction coefficients (see [2]) | $\alpha = 0.0$ |
| | $\alpha = 0.41$ km$^{-1}$ (1.8 dB/km) |
| background spectral radiance | $N_\lambda = 10$ W/m$^2$ SR μm |
| **Reciever Parameters** | |
| pupil diameter | $d_R = 0.5$ m |
| detector quantum efficiencies | $\eta_{APD} = 0.25$, $\eta_{PMT} = 0.005$ |
| load resistance | $R = 50\ \Omega$ |
| mean APD gain | $G = 100$ |
| load temperature | $T = 300^{o}$ K |
| optical filter bandwidth | $\Delta\lambda = 10^{-2}$ μm |
| receiver field-of-view cone angle | $d_D/\ell = 10^{-4}$ |
| **Target Parameters** | |
| area | $A_T = 10^{-2}$ m$^2$ |
| bidirectional reflectance | $\rho' = 10^{-1}$ |

fluctuation excess noise, and is strongly affected by thermal noise when $\alpha = 0.41$ km$^{-1}$ and $L > 5$ km.

Case 2 No Turbulence, Diffuse Target

For free-space propagation and a speckle target we find that

$$SNR^{o}_{sSAT} = \mathcal{D}^{o}, \tag{III.29}$$

and

$$SNR^{o}_{sq} = \eta P_T t_p (\pi d_T d_R / 4\lambda L)^2 A_T \times \tau_s (\lambda L \bar{f}_T)/h\nu_o L^2, \tag{III.30}$$

where the subscript "s" denotes speckle target. The $n_b$, $2kTt_p/Re^2G^2$ values for Case 1 apply here as well, thus, assuming $\tau_s = 0.1$ (arbitrarily) we get $SNR^{o}_{sq} = SNR^{o}_{gq}$ and the signal-to-noise ratio curves of Fig. 9. Comparing Figs. 8 and 9 shows that target fluctuations are the dominant performance limiting effect when $\alpha = 0.0$ with $1 \leq L \leq 10$ km, and when $\alpha = 0.41$ km$^{-1}$ with $1 \leq L \leq 3$ km.

Case 3 Turbulence, Specular Target

For a specular target viewed through atmospheric turbulence, we can show that

$$SNR_{gSAT} \approx 1/(e^{4\sigma_\chi^2} - 1), \tag{III.31}$$

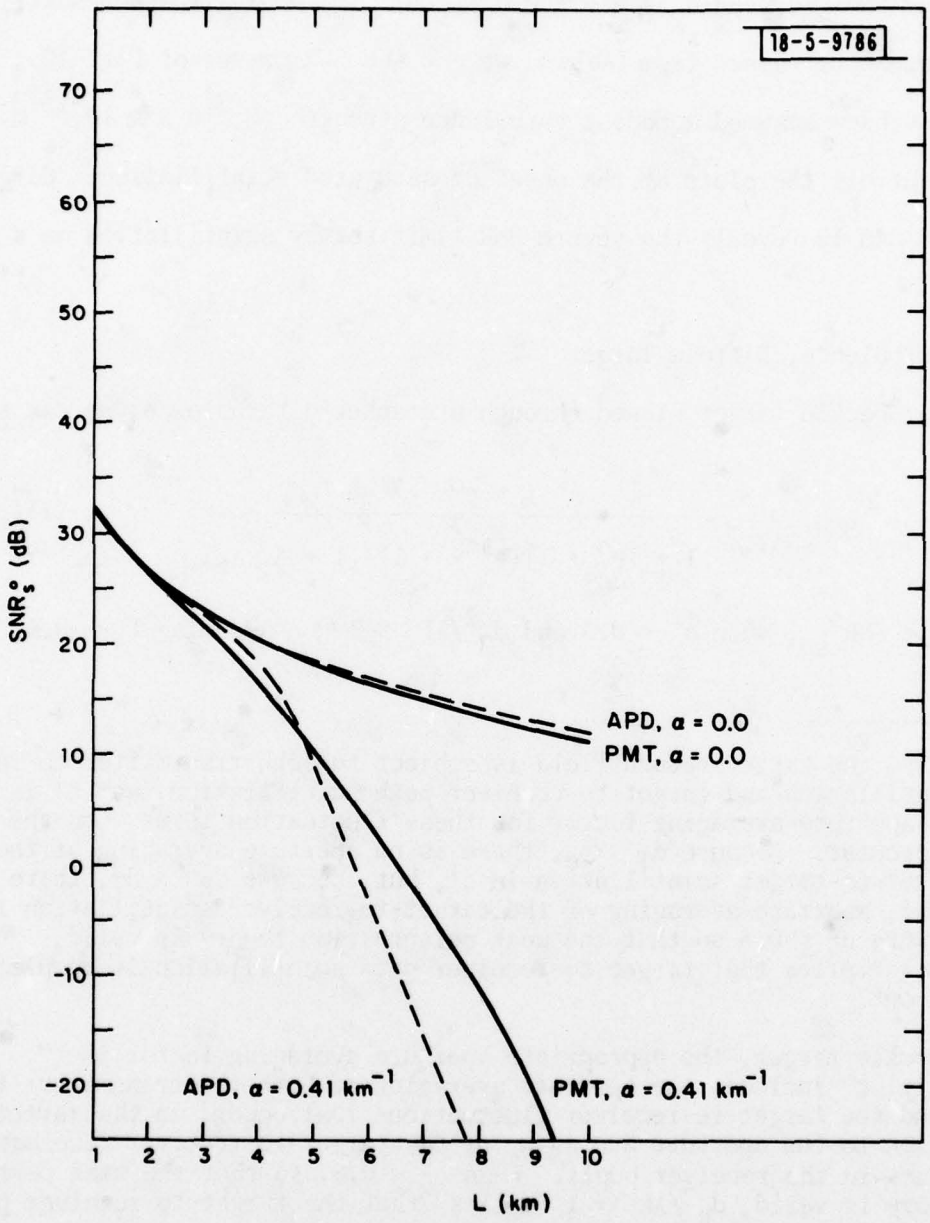


Fig.9. Free-space propagation speckle target signal-to-noise ratio vs path length L; Eqs.(III.8), (III.22), (III.29) and (III.30) are used with the parameters from Table 1 and $T_s$ = 0.1.

and $SNR_{gq} \approx SNR^{o}_{gq}$, when $\sigma_\chi^2 \leq 0.5$ and $d_R^2/\lambda L >> 1$*. Using these results and the parameter values from Table 1, we get the SNR curves of Fig. 10. In Fig. 10, we have assumed a modest turbulence strength ($C_n^2 = 5 \times 10^{-15}\ m^{-2/3}$), and have cut off the plots at the onset of saturated scintillation. Comparison of Figs. 8 and 10 reveals the severe SNR limit set by scintillation on a glint target.

Case 4 Turbulence, Diffuse Target

For a speckle target viewed through atmospheric turbulence, we can show that

$$SNR_{sSAT} \approx \frac{\mathcal{D}^o}{1 + (\mathcal{D}^o + 1)(e^{4\sigma_\chi^2} - 1)/(1 + A_T/\lambda L)} \qquad \text{(III.32)}$$

and $SNR_{sq} \approx SNR^{o}_{sq}$, when $\sigma_\chi^2 \leq 0.5$ and $d_R^2/\lambda L >> 1$**. Assuming $T_s = 0.1$, the

---

*Physically, the target-return field is subject to both transmitter-to-target path scintillation and target-to-receiver path scintillation, and $\zeta'$ is the relevant aperture-averaging factor for these fluctuation terms when the target is specular. Because $d_T < \rho_o$, there is no aperture averaging of the transmitter-to-target scintillation in $\zeta'$, but, because $d_R >> d_T$, there is, in general, aperture-averaging of the target-to-receiver scintillation in $\zeta'$. Indeed, when $\sigma_\chi^2 \leq 0.5$ so that the weak perturbation theory is valid, $d_R^2/\lambda L >> 1$ implies that target-to-receiver path scintillation is completely averaged out.

**For a speckle target, the appropriate aperture averaging factor is $\zeta''$. Physically, $\zeta''$ includes the aperture averaging of both the transmitter-to-target and the target-to-receiver fluctuations that occurs in the target plane, in addition to the aperture averaging of the target-to-receiver fluctuations that occurs in the receiver pupil. When $\sigma_\chi^2 < 0.5$, so that the weak perturbation theory is valid, $d_R^2/\lambda L >> 1$ implies that the target-to-receiver path scintillation is completely averaged out.

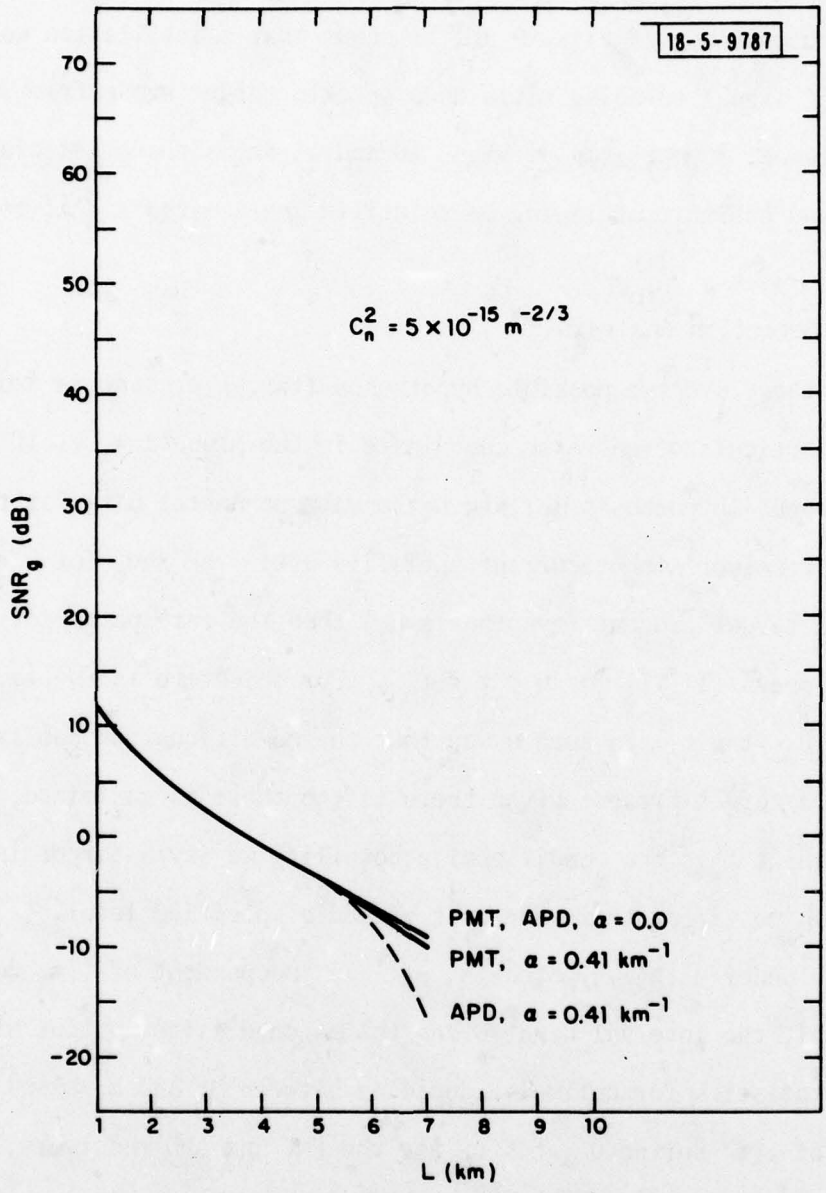


Fig.10. Atmospheric propagation glint target signal-to-noise ratio vs path length L; Eqs.(III.8), (III.22), and (III.31) are used with the parameter values from Table 1.

parameters of Table 1, and $C_n^2 = 5 \times 10^{-15}\ m^{-2/3}$ leads to the SNR curves of Fig. 11. Comparison of Figs. 9 and 11 shows that scintillation costs about 10 dB of signal-to-noise ratio on a speckle target whose free-space SNR exceeds 10 dB. Comparison of Figs. 10 and 11 shows the beneficial effect of target-plane aperture averaging on scintillation-limited signal-to-noise ratio.

## IV. Target-Detection Analysis

Suppose there are two possible hypotheses (target present or target absent at a particular transverse coordinate in the plane $z = L$). If no target is present (hypothesis $H_0$), then the rate parameter $\mu(t)$ for the (PMT or APD) receiver's photocurrent satisfies $\mu(t) = \eta P_b/h\nu_o$ for $0 \leq t \leq t_p$. If there is a target present (hypothesis $H_1$) then the rate parameter for the photocurrent obeys (II.11) for $0 \leq t \leq t_p$. Our objective is to process the data $\{i(t) : 0 \leq t \leq t_p\}$ in such a way that the conditional probability we say there is a target present given there is one there is maximized, subject to the constraint that the conditional probability we say a target is present given there is no target there does not exceed a specified level.

Because, under either hypothesis, $\mu(t)$ is independent of time during the pulse interval, the interval count N and the matched filter output N' are sufficient statistics for optimally deciding between $H_0$ and $H_1$ based on observation of $i(t)$ during $0 \leq t \leq t_p$ for the PMT and APD receivers, respectively. The structure and performance of the optimum PMT and APD receivers will be developed in this section.

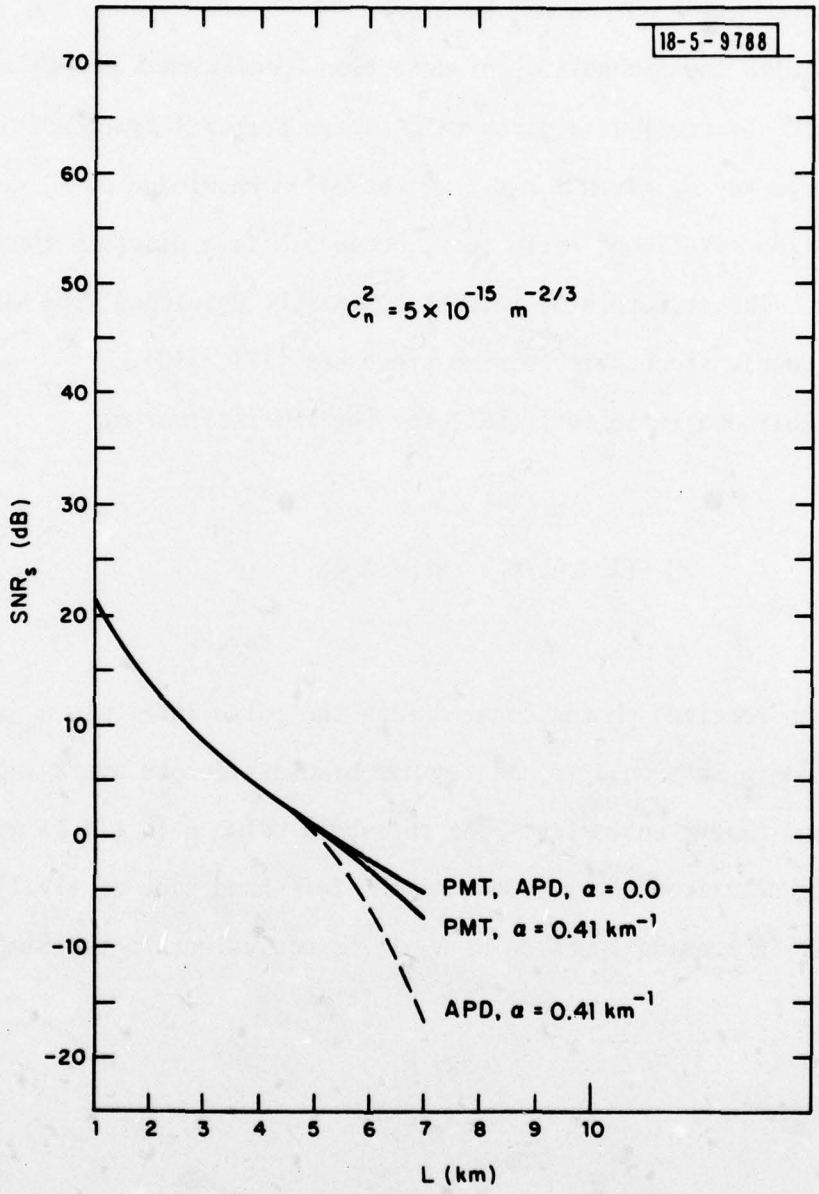


Fig.11. Atmospheric propagation speckle target signal-to-noise ratio; Eqs.(III.8), (III.22), and (III.32) are used with the parameters from Table 1 and $T_s = 0.1$.

IV.1 Target Detection with a PMT Receiver

To maximize the probability of detection (conditional probability you say $H_1$ given $H_1$ is true) at a given false alarm probability (conditional probability you say $H_1$ given $H_0$ is true) based on knowledge of N, we must use a randomized likelihood-ratio test, because N is a discrete random variable[16]. The structure of this test is easily developed from well known results for doubly stochastic Poisson processes [17], [18].

The likelihood-ratio test (LRT) for the PMT receiver is

$$\langle (1 + n_s/n_b)^N \exp(-n_s) \rangle \begin{array}{c} \text{say } H_1 \\ \geq \\ \leq \\ \text{say } H_0 \end{array} \tilde{\eta}, \qquad \text{(IV.1)}$$

where N is the received photon count during the pulse interval, $n_s$ and $n_b$ are as defined in Section III, and angular brackets denote averaging over the turbulence and target ensembles. The threshold value $\tilde{\eta}$ in (IV.1) will be determined as described later. Because the left-hand side of (IV.1) is a monotonically increasing function of N, it is equivalent to the simple threshold test

$$N \begin{array}{c} \text{say } H_1 \\ \geq \\ < \\ \text{say } H_0 \end{array} \gamma \qquad \text{(IV.2)}$$

where $\gamma$ is an integer chosen as described below. Note that the processor (IV.2) gives the LRT regardless of the strength of the turbulence, or whether the target is pure glint or pure speckle.

The receiver operating characteristic (ROC) for (IV.2) is a discrete set of points $\{(P_F(\gamma), P_D(\gamma)) : \gamma = 0, 1, 2, \ldots\}$ where $P_F(\gamma)$, $P_D(\gamma)$ denote the false-alarm and detection probabilities obtained by using (IV.2) with threshold $\gamma$. As shown in Fig. 12, a discrete ROC cannot provide a test which achieves maximum $P_D$ at arbitrary $P_F$ values [16]. Suppose, see Fig. 12, that p is the maximum allowed false-alarm probability and that $\gamma_p$ is a non-negative integer such that

$$P_F(\gamma_p) > p \geq P_F(\gamma_p + 1) \qquad \text{(IV.3)}$$

Using the randomized test, "say $H_1$ when $N \geq \gamma_p + 1$, say $H_0$ when $N < \gamma_p$, and when $N = \gamma_p$ say $H_1$ with probability $\beta$ and $H_0$ with probability $(1 - \beta)$" gives false-alarm probability $\beta P_F(\gamma_p) + (1 - \beta) P_F(\gamma_p + 1)$, and detection probability $\beta P_D(\gamma_p) + (1 - \beta) P_D(\gamma_p + 1)$; these probabilities appear as the straight line in Fig. 12 as $\beta$ varies from 0 to 1. It is clear from this line that choosing

$$\beta = (p - P_F(\gamma_p + 1))/(P_F(\gamma_p) - P_F(\gamma_p + 1)) \qquad \text{(IV.4)}$$

gives a test which has false-alarm probability exactly equal to p, and a higher detection probability than any LRT whose false-alarm probability is less than p; a more refined argument [16] shows that no test has a higher detection probability at false-alarm probability p or less.

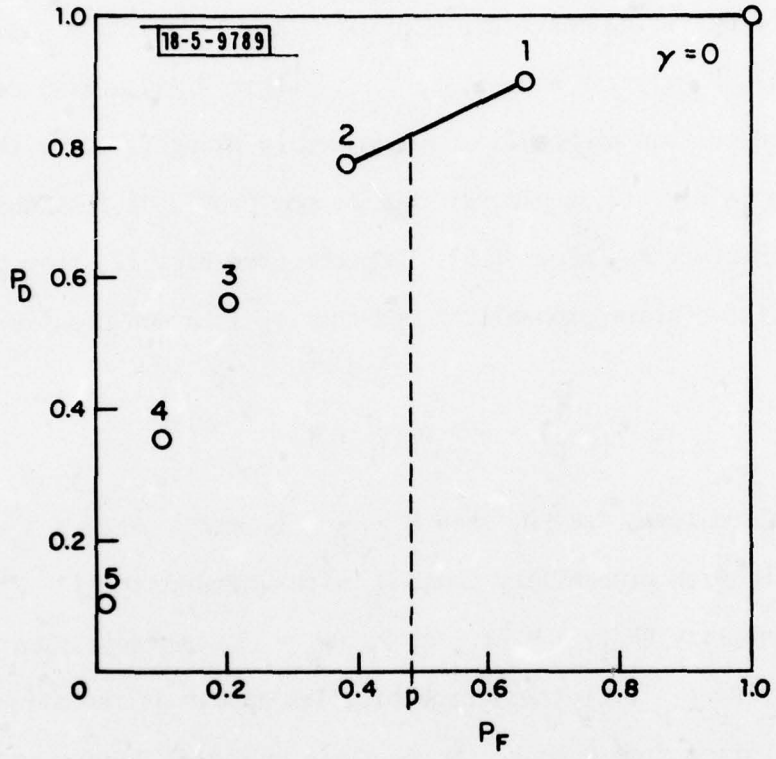


Fig.12. Illustration of a discrete random variable receiver operating characteristic; the open circles show $\{(P_F(\gamma), P_D(\gamma)): 0 \leq \gamma \leq 5\}$; the solid line is the randomized test performance for $\gamma_p = 1$; the intersection of the solid line with the $P_F = p$ line gives the maximum $P_D$ consistent with $P_F \leq p$.

The foregoing analysis, and Fig. 12 in particular, shows it suffices to derive the ROC $\{(P_F(\gamma), P_D(\gamma)) : \gamma = 0, 1, 2, \ldots\}$ to characterize the performance of the LRT (IV.2); randomized test performance is then found by connecting adjacent ROC points by straight line segments. It turns out to be relatively simple to deduce $(P_F(\gamma), P_D(\gamma))$ when the target is either specular or diffuse. Regardless of target and turbulence conditions, N is a Poisson random variable with mean $n_b$ under $H_0$. Thus, for any target/turbulence combination we find that

$$P_F(\gamma) = \sum_{n=\gamma}^{\infty} (n!)^{-1} (n_b)^n \exp(-n_b). \tag{IV.5}$$

The general expression for $P_D(\gamma)$ is

$$P_D(\gamma) = < \sum_{n=\gamma}^{\infty} (n!)^{-1} (n_s + n_b)^n \exp[-(n_s + n_b)] >, \tag{IV.6}$$

where angular brackets denote averaging over the turbulence and target ensembles. More explicit results are developed below.

Case 1 Specular Target

For a specular target, we find, from (III.3), (III.4), (III.12), that

$$n_s = < n_s >_g e^{2w}, \tag{IV.7}$$

where

$$e^{2w} \equiv \frac{\int d\bar{\rho}\ \text{circ}\ (2|\bar{\rho}|/d_R)\ \exp[2\chi(\bar{\rho}_g', \bar{0}) + 2\chi(\bar{\rho}_g', \bar{\rho})]}{\int d\bar{\rho}\ \text{circ}\ (2|\bar{\rho}|/d_R)\ \exp(4C_{\chi\chi}(\bar{0}, \bar{\rho}))} . \quad \text{(IV.8)}$$

Because $\chi(\bar{\rho}', \bar{\rho})$ is a Gaussian process, and sums of real-valued lognormal random variables are themselves approximately lognormal random variables [19], [20], we have that w is a Gaussian random variable. By direct calculation of the variance of $n_s$ it follows that w has mean $-\sigma'^2$ and variance $\sigma'^2$ where

$$e^{4\sigma'^2} - 1 = \zeta'(e^{16\sigma_\chi^2} - 1) \quad \text{(IV.9)}$$

and $\zeta'$ is given by (III.16). Thus, the glint-target PMT receiver detection probability satisfies

$$P_D(\gamma)_g = \int_{-\infty}^{\infty} dW\ p_w(W)\ P_D^{\,o}\ (\gamma;\ <n_s>_g e^{2W},\ n_b)_g \quad \text{(IV.10)}$$

with $p_w(W) = (2\pi\sigma'^2)^{-1/2}\ \exp[-(W + \sigma'^2)^2/2\sigma'^2]$, and

$$P_D^{\,o}(\gamma;\ a,\ b)_g = \sum_{n=\gamma}^{\infty} (n!)^{-1}\ (a + b)^n\ \exp[-(a + b)]. \quad \text{(IV.11)}$$

The quantity $P_D^{\,o}(\gamma;\ a,\ b)_g$ given by (IV.11) is the glint-target free-space detection probability achieved by the test (IV.2) when the average target return count is a and the average background count is b. Equation (IV.10) shows, therefore, that the presence of turbulence introduces a lognormal fading into the detection probability calculation.

Case 2 Diffuse Target

For a diffuse target, (III.3) shows that $\underline{E}_R(\bar{\rho})$ is a circulo-complex Gaussian random process conditioned on knowledge of $\chi$, $\phi$. By means of the equal-eigenvalue approximation, we then have the conditional counting distribution [21]-[23].

$$\Pr[N = n \mid \chi, \phi, H_1] \approx$$

$$[(\bar{n}_s/\mathcal{D})^n/(1 + \bar{n}_s/\mathcal{D})^{n+\mathcal{D}}] \exp[-n_b/(1 + \bar{n}_s/\mathcal{D})]$$

$$\times L_n^{\mathcal{D}-1}[-n_b\mathcal{D}/\bar{n}_s(1 + \bar{n}_s/\mathcal{D})], \qquad \text{(IV.12)}$$

where

$$\bar{n}_s = (\eta P_T t_p/h\nu_o L^2) \mid \underline{\xi}_t(\lambda L\bar{f}_T)\mid^2 T_s(\lambda L\bar{f}_T)$$

$$\times \int d\bar{\rho}\ \text{circ}\ (2|\bar{\rho}|/d_R) \int d\bar{\rho}'\ \exp[2\chi(\bar{\rho}', \bar{0}) + 2\chi(\bar{\rho}', \bar{\rho})], \qquad \text{(IV.13)}$$

is the average number of counts due to the diffuse target conditioned on knowledge of the turbulence parameters. In Eq. (IV.12) $L_n^{\mathcal{D}-1}$ is the generalized Laguerre polynomial of index n and order $\mathcal{D} - 1$, i.e.,

$$L_n^{\mathcal{D}-1}(x) = \sum_{i=0}^{n} \binom{n+\mathcal{D}-1}{i} (-x)^i/i!, \qquad \text{(IV.14)}$$

and $\mathcal{D}$ is the number of degrees of freedom of the observation [22]. Strictly speaking, $\mathcal{D}$ is a function of the turbulence parameters $\chi$ and $\phi$; this makes

) over the turbulence ensemble e[illegible]emely dif-
asonable approximation [24], that [illegible] given
space value $D^o$, which, for a target [illegible] lies
T - diameter illumination region, satis[illegible]s (III.18).
ore the convergence properties of sums of [illegible]normal
may express $\bar{n}_s$ in the form

$$\bar{n}_s = \langle n_s \rangle_s e^{2V} \tag{IV.15}$$

aussian random variable with mean $-\sigma''^2$ and varianc[illegible]$\sigma''^2$, and

$$e^{4\sigma''^2} - 1 \equiv \zeta''(e^{16\sigma_\chi^2} - 1). \tag{IV.16}$$

e that the speckle-target PMT receiver detection probab[illegible]ty is

$$P_D(\gamma) = \int_{-\infty}^{\infty} dV p_V(V)\, P_D^o(\gamma;\, \langle n_s \rangle_s e^{2V},\, n_b)_s, \tag{IV.17}$$

re $p_V(V) = (2\pi\sigma''^2)^{-1/2} \exp[-(V + \sigma''^2)^2/2\sigma''^2]$, and

$$P_D^o(\gamma;\, a,\, b)_s = \sum_{n=\gamma}^{\infty} [(a/D^o)^n / [illegible]^{n+1}]\, D^o\, ]\, \exp[-b/(1 + [illegible]D^o)] \tag{IV.18}$$

[illegible]$^{-bD^o}/a(1 + a/D^o)]$,

is the f[illegible]ce speckle target PMT receiver detection probability [illegible]n a is
the [illegible]rage target-return count and b is the average background coun[illegible]er
Calculations are available [22], [25] for the free-space PMT rec[illegible]given
ROC, for both pure glint and pure speckle targets; some examples will

subsequent averaging of (IV.12) over the turbulence ensemble extremely difficult. We shall use the reasonable approximation [24], that $\mathcal{D}$ is given approximately by its free-space value $\mathcal{D}^o$, which, for a target that lies entirely within the $\lambda L/d_T$ - diameter illumination region, satisfies (III.18).

Now, using once more the convergence properties of sums of lognormal random variables, we may express $\bar{n}_s$ in the form

$$\bar{n}_s = \langle n_s \rangle_s e^{2v} \tag{IV.15}$$

where v is a Gaussian random variable with mean $-\sigma''^2$ and variance $\sigma''^2$, and

$$e^{4\sigma''^2} - 1 \equiv \zeta''(e^{16\sigma_\chi^2} - 1). \tag{IV.16}$$

We now have that the speckle-target PMT receiver detection probability is

$$P_D(\gamma) = \int_{-\infty}^{\infty} dV p_v(V)\ P_D^{\,o}\ (\gamma;\ \langle n_s \rangle_s e^{2V},\ n_b)_s, \tag{IV.17}$$

where $p_v(V) = (2\pi\sigma''^2)^{-1/2}\ \exp[-(V + \sigma''^2)^2/2\sigma''^2]$, and

$$P_D^{\,o}\ (\gamma;\ a,\ b)_s = \sum_{n=\gamma}^{\infty} [(a/\mathcal{D}^o)^n/(1 + a/\mathcal{D}^o)^{n+\mathcal{D}^o}]\ \exp[-b/(1 + a/\mathcal{D}^o)]$$

$$\times L_n^{\mathcal{D}^o - 1}\ [-b\mathcal{D}^o/a(1 + a/\mathcal{D}^o)], \tag{IV.18}$$

is the free-space speckle target PMT receiver detection probability when a is the average target-return count and b is the average background count.

Calculations are available [22], [25] for the free-space PMT receiver ROC, for both pure glint and pure speckle targets; some examples will be given

after we analyze the ROC for APD reception. Calculations have yet to be done for the PMT receiver ROC in the presence of turbulence.

IV.2 Target Detection with an APD Receiver

Well known results for Gaussian detection [15] permit us to show that the likelihood-ratio test based on the observation of N' is

$$\begin{aligned} &\langle [1 + n_s/(n_b + 2kTt_p/Re^2G^2F)]^{-1/2} \\ &\quad \times \exp\{-[N' - (n_s + n_b)]^2/2[(n_s + n_b)F + 2kTt_p/Re^2G^2] \\ &\qquad + (N' - n_b)^2/2[n_bF + 2kTt_p/Re^2G^2]\}\rangle \\ &\qquad \begin{array}{l} \text{say } H_1 \\ \geq \\ \\ < \\ \text{say } H_0 \end{array} \quad \tilde{\eta} \end{aligned} \tag{IV.19}$$

where angular brackets denote averaging over the target and turbulence ensembles, and the threshold $\tilde{\eta}$ is chosen to achieve the false alarm probability constraint with equality.

It turns out that the left member of (IV.19) is a monotonically increasing function of N', thus (IV.19) can be reduced to the simple threshold test

$$N' \begin{array}{l} \text{say } H_1 \\ \geq \\ < \\ \text{say } H_0 \end{array} \gamma, \tag{IV.20}$$

where $\gamma$ is chosen to satisfy the false alarm constraint with equality. This test is the optimum processor for all target/turbulence combinations.

For the test (IV.20), it is easy to find the false-alarm probability $P_F$, because under $H_0$ N' is a Gaussian random variable with mean $n_b$ and variance $\sigma_0^2 \equiv n_b F + 2kTt_p/Re^2G^2$. Thus for all target and turbulence conditions we find that

$$P_F = Q[(\gamma - n_b)/\sigma_0], \tag{IV.21}$$

where $Q(x) = (2\pi)^{-1/2} \int_x^\infty dy \exp(-y^2/2)$ is the area under the tail of the normalized Gaussian density. Equation (IV.21) can be inverted numerically to obtain $\gamma$ as a function of $P_F$, $n_b$ and $\sigma_0$.

The general result for the detection probability $P_D$ is obtained by noting that given $\underline{T}$, $\chi$, $\phi$, $H_1$, the random variable N' is Gaussian with mean $n_s + n_b$ and variance $\sigma_1^2 \equiv (n_s + n_b) F + 2kTt_p/Re^2G^2$, whence

$$P_D = \langle Q[(\gamma - (n_s + n_b))/\sigma_1] \rangle. \tag{IV.22}$$

In what follows we consider the pure glint and pure speckle limits of (IV.22).

Case 1 Specular Target

For a specular target, we have that $n_s = \langle n_s \rangle_g e^{2W}$, from (IV.7). This tells us that the glint-target APD receiver detection probability obeys

$$P_D(\gamma)_g = \int_{-\infty}^{\infty} dW p_w(W)\, Q[(\gamma - (\langle n_s \rangle_g e^{2W} + n_b))/\sigma_1(W)], \tag{IV.23}$$

where $p_w(W) = (2\pi\sigma'^2)^{-1/2} \exp[-(W + \sigma'^2)^2/2\sigma'^2]$ as before, and $\sigma_1^2(W) = (<n_s>_g e^{2W} + n_b) F + 2kTt_p/Re^2G^2$.

Case 2 Diffuse Target

By means of the equal-eigenvalue approximation, with the number of free-space degrees of freedom $\mathcal{D}^o$ used in place of the number of atmospheric degrees of freedom $\mathcal{D}$, we can show that the speckle-target count parameter $n_s$ is given by

$$n_s = <n_s>_s m e^{2v}, \tag{IV.24}$$

for v is as in Section IV.1, and m a random variable that is statistically independent of v with density function

$$p_m(M) = [\mathcal{D}^o(\mathcal{D}^o M)^{\mathcal{D}^o - 1}/(\mathcal{D}^o - 1)!] \exp(-\mathcal{D}^o M)\, u(M), \tag{IV.25}$$

where u(M) is the unit step function. Thus, the speckle-target APD receiver detection probability is

$$P_D(\gamma)_s = \int_{-\infty}^{\infty} dV p_v(V) \int_{-\infty}^{\infty} dM p_m(M) \times Q[(\gamma - (<n_s>_s M e^{2V} + n_b))/\sigma_1(M, V)] \tag{IV.26}$$

where $\sigma_1^2(M, V) = (<n_s>_s M e^{2V} + n_b) F + 2kTt_p/Re^2G^2$.

As yet ROC calculations are not available for the APD receiver, except when it is thermal-noise or background shot-noise limited [15], [26].

IV.3 ROC Examples

The numerical evaluation of the foregoing ROC results is presently underway, and will be the subject of a subsequent report. In this section,

we shall present some simple free-space performance results.

Case 1 No Turbulence, Specular Target

In the absence of turbulence, the PMT receiver glint-target detection probability is given by (IV.11) and the randomized test procedure (IV.3), (IV.4). We have plotted this detection probability in Fig. 13 for several false-alarm rates with $n_b = 0.0$ and $n_b = 0.2$. In this figure, we have used $SNR^o_{gq}$ in lieu of $\langle n_s \rangle_g$ to facilitate obtaining detection probabilities for the parameters given in Table 1 via Fig. 7. We see that, for the parameters given in Table 1, a 95% detection probability can be maintained with $P_F = 10^{-6}$ out to a 5 km path length when $\alpha = 0.41$ km$^{-1}$.

The APD receiver free-space glint-target detection probability, obtained from (IV.23) with $\sigma'^2 = 0$, is shown in Fig. 14 for several false-alarm rates, assuming the parameters of Table 1. We see, from Figs. 7, 14 that the APD system can achieve $P_D = 0.95$, $P_F = 10^{-6}$ almost out to L = 5 km when $\alpha = 0.41$ km$^{-1}$. This is so because the 17 dB $SNR_q$ advantage of the APD receiver just about balances out its thermal-noise performance degradation

Case 2 No Turbulence, Diffuse Target

In Fig. 15 we have plotted the free-space speckle-target PMT receiver detection probability, assuming no background noise, for several degrees of freedom values. Comparison of Figs. 13 and 15 shows that when $\mathcal{D}^o = 1$ we need about an 8 db $SNR^o_q$ increase to maintain $P_D = 0.95$. On the other hand, for $\mathcal{D}^o = 10^2$ speckle target and glint target performance are virtually identical. The latter result is a manifestation of the constant-intensity (low photon coherence) limit [21], [22], which is also valid in the presence

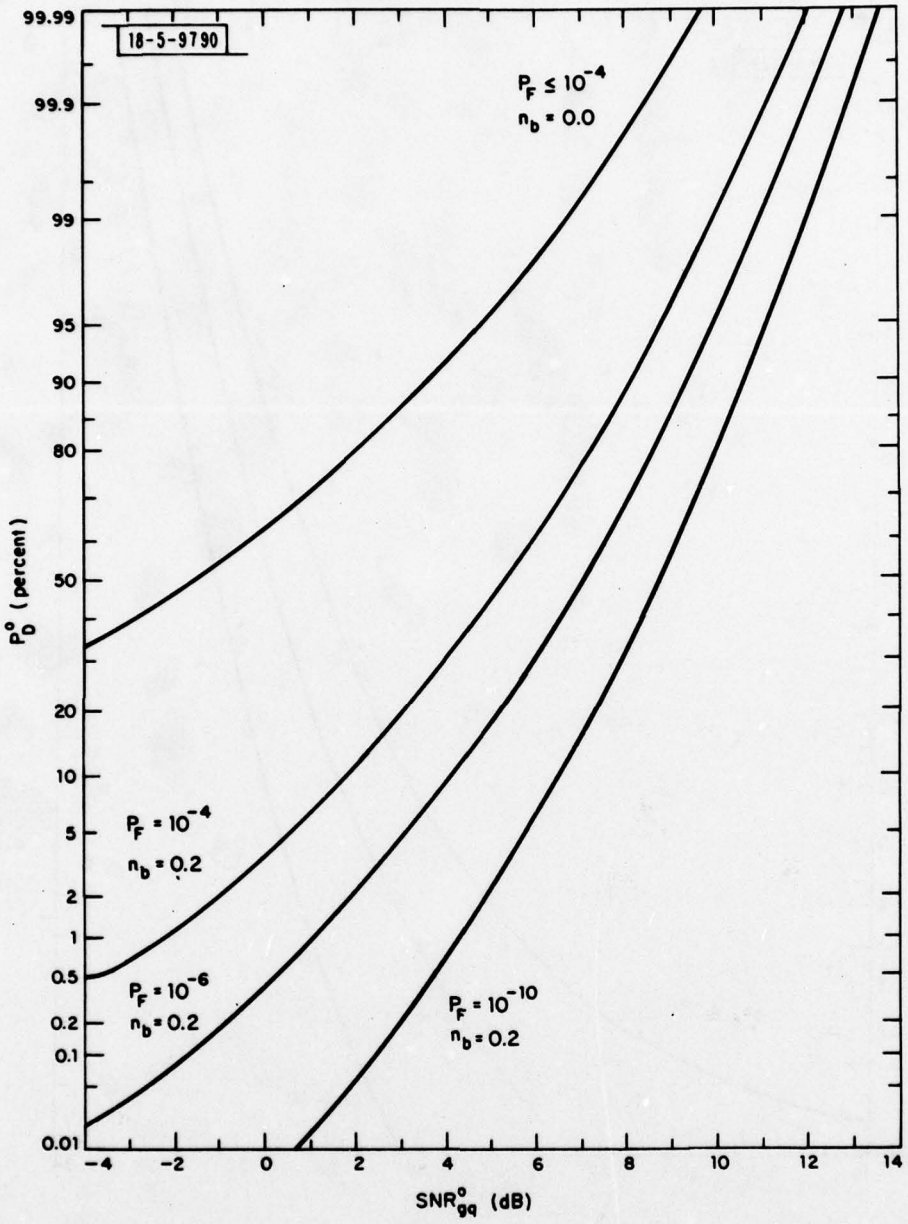


Fig.13. Free-space propagation glint target detection probability for the PMT receiver vs quantum limited signal-to-noise ratio.

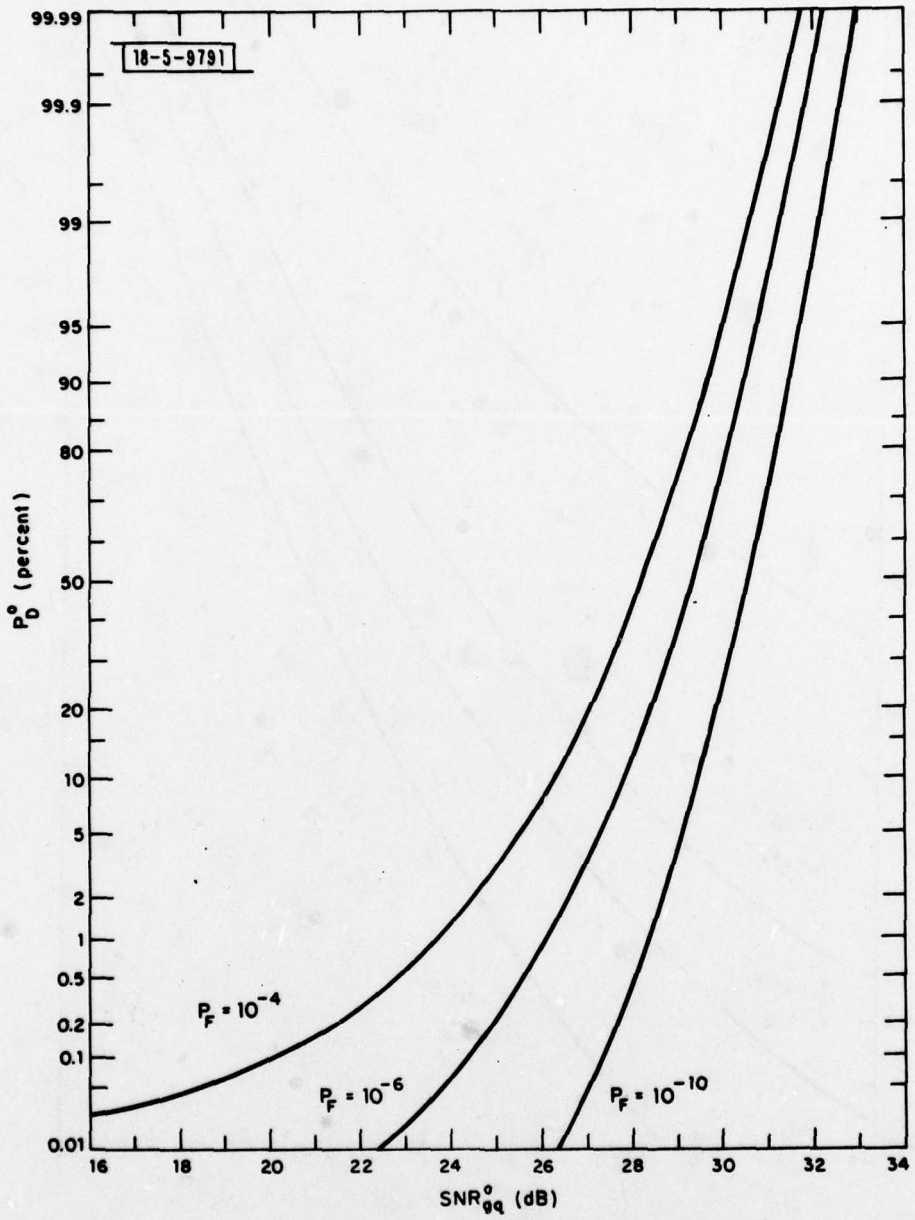


Fig.14. Free-space propagation glint target detection probability for the APD receiver vs quantum limited signal-to-noise; the parameter values from Table 1 are used in calculating the background and thermal noise levels.

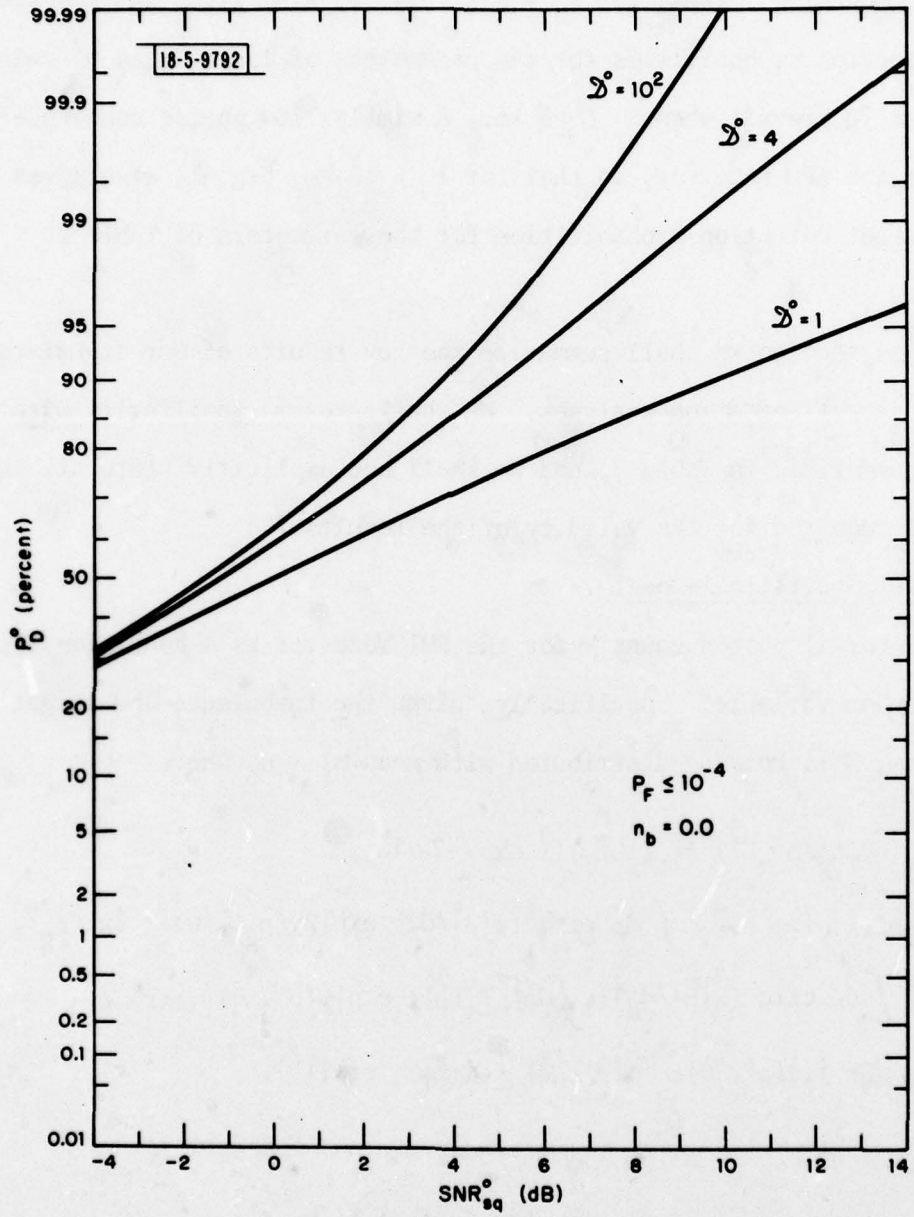


Fig.15. Free-space propagation speckle target detection probability vs quantum limited signal-to-noise ratio.

of background noise. Thus, for $n_b = 0.2$, Fig. 13 also gives the speckle target detection probabilities for the parameters of Table 1, as $\mathcal{D}^o$ values of at least 70 prevail when $1 \leq L \leq 5$ km. A similar low photon coherence limit exists for the APD receiver, so that for $1 \leq L \leq 5$ km, Fig. 14 also gives the speckle target detection probabilities for the parameters of Table 1.

## V. Summary

In this section we shall summarize the key results of our signal-to-noise ratio and target detection analyses. We shall presume familiarity with the notation summarized in Table 2, and we shall not explicitly state all the conditions required for the validity of the results.

### PMT-Receiver Statistical Model

The interval photon count N for the PMT receiver is a conditionally-Poisson random variable. Specifically, given the turbulence and target characteristics, N is Poisson-distributed with mean $n_s + n_b$ where

$$n_s = (\eta P_T t_p / h\nu_o L^2) \, |\underline{\xi}_t(\lambda L \bar{f}_T)|^2 \exp(-2\alpha L)$$
$$\times \{A_T \rho'(\lambda; \bar{f}_T; -\bar{f}_T) \int d\bar{\rho} \, \mathrm{circ}\,(2|\bar{\rho}|/d_R) \exp[2\chi(\bar{\rho}_g', \bar{0}) + 2\chi(\bar{\rho}_g', \bar{\rho})]$$
$$+ \lambda^{-2} \int d\bar{\rho} \, \mathrm{circ}\,(2|\bar{\rho}|/d_R) \left| \int d\bar{\rho}' \, \underline{T}_s(\bar{\rho}') \exp[\chi(\bar{\rho}', \bar{0}) + \chi(\bar{\rho}', \bar{\rho}) \right.$$
$$\left. + j(\phi(\bar{\rho}', \bar{0}) - \phi(\bar{\rho}', \bar{\rho}) + 4\pi \bar{f}_T \cdot \bar{\rho}')] \right|^2 \}, \qquad (V.1)$$

and

$$n_b = \eta \lambda^2 \Delta\lambda N_\lambda \, (\pi d_R d_D / 4\lambda\ell)^2 t_p / h\nu_o. \qquad (V.2)$$

TABLE 2

SUMMARY OF NOTATION

Radar Parameters

$P_T$ = transmitter peak power

$t_p$ = pulse duration

$d_T$ = transmitter optics diameter

$d_R$ = receiver optics diameter

$\lambda$ = 1.06 μm wavelength

$h\nu_o$ = photon energy at 1.06 μm wavelength

$\eta$ = detector quantum efficiency

R = APD load resistor

G = APD current gain

F = APD excess-noise factor

kT = thermal energy

$\Delta\lambda$ = optical filter bandwidth

$d_D/\ell$ = receiver field-of-view cone angle

$\underline{\xi}_t$ = normalized target-plane illumination beam

Atmospheric Parameters

$\chi$ = turbulence-induced log-amplitude fluctuation

$\phi$ = turbulence-induced phase fluctuation

L = path length

$\sigma_\chi^2$ = log-amplitude variance

TABLE 2 (Continued)

$\alpha$ = extinction coefficient

$\zeta'$, $\zeta''$ = aperture-averaging factors

$\sigma'^2$, $\sigma''^2$ = aperture averaged log-amplitude variances

$N_\lambda$ = background-light spectral radiance

Target Parameters

$A_T$ = target area

$T_s$ = diffuse-reflection coefficient

$\rho'(\lambda; \bar{f}_T; -\bar{f}_T)$ = target bidirectional reflectance for a glint return

$T_s$ = average diffuse reflection coefficient

$\mathcal{D}^o$ = free-space propagation speckle target degrees of freedom

APD-Receiver Statistical Model

The matched-filter output N' for the APD receiver is assumed to be Gaussian-distributed, given the turbulence and target characteristics, with mean $n_s + n_b$, and variance $F(n_s + n_b) + 2kTt_p/Re^2G^2$.

Receiver Signal-to-Noise Ratio

The receiver signal-to-noise ratios defined by

$$SNR_{PMT} \equiv \frac{(<N> - n_b)^2}{Var(N)} \tag{V.3}$$

and

$$SNR_{APD} = \frac{(<N'> - n_b)^2}{Var(N')} \tag{V.4}$$

can both be put into the standard form

$$SNR = \frac{SNR_q}{F' + SNR_q/SNR_{SAT} + F'(SBR)^{-1} + \delta_{FF'}(STR)^{-1}} \tag{V.5}$$

by the following identifications:

quantum-limited signal-to-noise ratio

$$SNR_q = <n_s> ; \tag{V.6}$$

excess-noise factor

$$F' = \begin{cases} 1, & \text{for PMT reception} \\ F, & \text{for APD reception;} \end{cases} \tag{V.7}$$

saturation signal-to-noise ratio

$$SNR_{SAT} = <n_s>^2/Var(n_s); \tag{V.8}$$

signal-to-background ratio

$$SBR = \langle n_s \rangle / n_b; \tag{V.9}$$

and signal-to-thermal ratio

$$STR = \langle n_s \rangle \, Re^2 G^2 / 2kTt_p \tag{V.10}$$

At very low $SNR_q$ values, (V.5) shows that performance is background and/or thermal noise limited; in this regime the SNR increases as the square of $SNR_q$. For $SNR_q$ values large enough to give STR $\geq$ 10/F' and SBR $\geq$ 10, (V.5) reduces to the universal curve (Fig. 5).

$$\frac{SNR}{SNR_{SAT}} \approx \frac{SNR_q/SNR_{SAT}}{F' + SNR_q/SNR_{SAT}} \tag{V.11}$$

Increasing $SNR_q$ beyond $F'SNR_{SAT}$ does little, therefore, to improve receiver signal-to-noise ratio.

The foregoing signal-to-noise ratio results have the following behavior in particular cases of interest:

i) No Turbulence, Specular Target (Figs. 7, 8)

$$SNR^o_{gq} = \eta P_T t_p (\pi d_T d_R / 4\lambda L)^2 \, A_T \exp(-2\alpha L) \times \rho'(\lambda; \bar{f}_T; -\bar{f}_T)/h\nu_o L^2, \tag{V.12}$$

$$SNR^o_{gSAT} = \infty \tag{V.13}$$

ii) No Turbulence, Diffuse Target (Figs. 7, 9)

$$SNR^{o}_{sq} = \eta P_T t_p (\pi d_T d_R / 4\lambda L)^2 A_T \exp(-2\alpha L)$$

$$x\ T_s(\lambda L \bar{f}_T)/h\nu_o L^2, \tag{V.14}$$

$$SNR^{o}_{sSAT} = \mathcal{D}^{o} \tag{V.15}$$

iii) Turbulence, Specular Target (Figs. 7, 10)

$$SNR_{gq} \approx SNR^{o}_{gq}, \tag{V.16}$$

$$SNR_{gSAT} \approx 1/(e^{4\sigma_\chi^2} - 1). \tag{V.17}$$

iv) Turbulence, Diffuse Target (Figs. 7, 11)

$$SNR_{sq} \approx SNR^{o}_{sq} \tag{V.18}$$

$$SNR_{sSAT} \approx \frac{\mathcal{D}^{o}}{1 + (\mathcal{D}^{o} + 1)(e^{4\sigma_\chi^2} - 1)/(1 + A_T/\lambda L)} \tag{V.19}$$

Likelihood-Ratio Tests

The PMT-receiver decision rule which maximizes the conditional probability you say a target is present given there is one present, subject to the constraint that the conditional probability you say a target is present given there is no target there does not exceed p, is the randomized test:

i) $N \geq \gamma_p + 1$, say $H_1$

ii) $N = \gamma_p$, say $H_1$ with probability $\beta$ and $H_0$ with probability $(1 - \beta)$

iii) $N < \gamma_p$, say $H_0$, where $\gamma_p$ is the integer which satisfies

$$\sum_{n=\gamma_p}^{\infty} (n!)^{-1} n_b^n e^{-n_b} > p \geq \sum_{n=\gamma_p+1}^{\infty} (n!)^{-1} n_b^n e^{-n_b}$$

for p = the maximum allowed false-alarm probability, and

$$\beta = [p - \sum_{n=\gamma_p+1}^{\infty} (n!)^{-1} n_b^n e^{-n_b}]/(\gamma_p!)^{-1} n_b^{\gamma_p} e^{-n_b}.$$

The APD-receiver decision rule which is optimum under the foregoing detection probability criterion is the threshold test

$$N' \underset{\text{say } H_0}{\overset{\text{say } H_1}{\gtrless}} \gamma , \tag{V.20}$$

where $\gamma$ is chosen to satisfy

$$p = Q[(\gamma - n_b)/(n_b F + 2kTt_p/Re^2G^2)^{1/2}]$$

for p = the maximum allowed false-alarm probability, and $Q(x) = (2\pi)^{-1/2} \cdot \int_x^{\infty} dy \exp(-y^2/2)$.

Receiver Operating Characteristics

For the PMT-receiver, the randomized threshold test gives detection probability

$$P_D = \beta P_D(\gamma_p) + (1-\beta) P_D(\gamma_p + 1) \tag{V.21}$$

where $P_D(\gamma)$ is the detection probability for the threshold test

$$N \underset{<}{\overset{\text{say } H_1}{\geq}} \gamma, \ \gamma \text{ an integer} \quad \text{say } H_0 \tag{V.22}$$

The behavior of $P_D(\gamma)$ is as follows

i) No Turbulence, Specular Target (Fig. 13)

$$P_D^o(\gamma) = P_D^o(\gamma; SNR_{gq}^o, n_b)_g \tag{V.23}$$

where $P_D^o(\gamma; a, b)_g = \sum_{n=\gamma}^{\infty} (n!)^{-1} (a+b)^n \exp[-(a+b)]$.

ii) No Turbulence, Diffuse Target (Fig. 15)

$$P_D^o(\gamma) = P_D^o(\gamma; SNR_{sq}^o, n_b)_s \tag{V.24}$$

where

$$P_D^o(\gamma; a, b)_s = \sum_{n=\gamma}^{\infty} [(a/\mathcal{D}^o)^n/(1+a/\mathcal{D}^o)^{n+\mathcal{D}^o}] \exp[-b/(1+a/\mathcal{D}^o)]$$

$$\times L_n^{\mathcal{D}^o - 1}[-b\mathcal{D}^o/a(1+a/\mathcal{D}^o)].$$

iii) Turbulence, Specular Target

$$P_D^o(\gamma) = \int_{-\infty}^{\infty} dW p_w(W)\, P_D^o(\gamma;\ SNR_{gq}\, e^{2W},\ n_b)_g, \tag{V.25}$$

where

$$p_w(W) = (2\pi\sigma'^2)^{-1/2} \exp[-(W+\sigma'^2)^2/2\sigma'^2],$$

with $e^{4\sigma'^2} - 1 = \zeta'(e^{16\sigma_\chi^2} - 1)$.

iv) Turbulence, Diffuse Target

$$P_D(\gamma) = \int_{-\infty}^{\infty} dV p_v(V)\, P_D^o(\gamma;\ SNR_{sq}\, e^{2V},\ n_b)_s, \tag{V.26}$$

where

$$p_v(V) = (2\pi\sigma''^2)^{-1/2} \exp[-(V+\sigma''^2)^2/2\sigma''^2]$$

with $e^{4\sigma''^2} - 1 = \zeta''(e^{16\sigma_\chi^2} - 1)$.

For the APD reciever, the threshold test (V.20) gives the following detection probabilities:

i) No Turbulence, Specular Target (Fig. 14)

$$P_D^o = Q[(\gamma - SNR_{gq}^o - n_b)/\sigma_1], \tag{V.27}$$

with $\sigma_1^2 = F(SNR_{gq}^o + n_b) + 2kTt_p/Re^2G^2$.

ii) No Turbulence, Diffuse Target

$$P_D^o = \int_{-\infty}^{\infty} dM p_m(M)\, Q[(\gamma - SNR_{sq}^o\, M - n_b)/\sigma_1(M)] \tag{V.28}$$

with $\sigma_1^2(M) = F(SNR_{sq}^o\, M + n_b) + 2kTt_p/Re^2G^2$,

and $p_m(M) = [\mathcal{D}^o(\mathcal{D}^oM)^{\mathcal{D}^o - 1}/(\mathcal{D}^o - 1)!] \exp(-\mathcal{D}^oM)\ u(M)$.

iii) Turbulence, Specular Target

$$P_D = \int_{-\infty}^{\infty} dW p_w(W)\, Q\left[(\gamma - SNR_{gq}\, e^{2W} - n_b)/\sigma_1(W)\right] \qquad (V.29)$$

where $\sigma_1^2(W) = F(SNR_{gq}\, e^{2W} + n_b) + 2kTt_p/Re^2G^2$.

iv) Turbulence, Diffuse Target

$$P_D = \int_{-\infty}^{\infty} dV \int_{-\infty}^{\infty} dM p_v(V)\ p_m(M)\, Q\left[(\gamma - SNR_{sq}\, Me^{2V} - n_b)/\sigma_1(M, V)\right], \qquad (V.30)$$

where $\sigma_1^2(M, V) = F(SNR_{sq}\, Me^{2V} + n_b) + 2kTt_p/Re^2G^2$.

## ACKNOWLEDGMENTS

In preparing this report, the author benefited from the encouragement of A. B. Gschwendtner and H. Kleiman, and useful technical discussions with R. C. Harney. Their support and guidance have made this study possible.

## REFERENCES


1. J. H. Shapiro, "Imaging and Target Detection with a Heterodyne-Reception Optical Radar," Project Report TST-24, Lincoln Laboratory, M.I.T. (13 October 1978).

2. R. J. Becherer, "Pulsed Laser Ranging Techniques at 1.06 and 10.6 μm," Project Report TT-8, Lincoln Laboratory, M.I.T. (19 March 1976), DDC AD-A024557/1.

3. E. V. Hoversten, "Optical Communication Theory," in Laser Handbook, F. T. Arecchi and E. O. Schulz-DuBois, Eds. (North-Holland, Amsterdam, 1972).

4. D. L. Snyder, Random Point Processes (Wiley, New York, 1975), Chap. 2.

5. R. M. Gagliardi and S. Karp, Optical Communications (Wiley, New York, 1976), Chap. 3.

6. J. H. Shapiro, "Imaging and Optical Communication through Atmospheric Turbulence," in Laser Beam Propagation through the Atmosphere, J. W. Strohbehn, Ed. (Springer-Verlag, Berlin, 1978).

7. W. K. Pratt, Laser Communication Systems (Wiley, New York, 1969), Chap. 6.

8. N. S. Kopeika and J. Bordogna, "Background Noise in Optical Communication Systems," Proc. IEEE 58, 1571-1577 (1970).

9. S. D. Personick, "New Results on Avalanche Multiplication Statistics with Applications to Optical Detection," Bell Syst. Tech. J. 50, 167-189 (1971).

10. S. D. Personick, "Statistics of a General Class of Avalanche Detectors with Applications to Optical Communication," Bell Syst. Tech. J. 50, 3075-3095 (1971).

11. S. D. Personick, P. Balaban, J. H. Bobsin and P. R. Kumar, "A Detailed Comparison of Four Approaches to the Calculation of the Sensitivity of Optical Fiber System Receivers," IEEE Trans. Commun. COM-25, 541-548 (1977).

12. S. D. Personick, "Receiver Design for Digital Fiber Optic Communication Systems," Bell Syst. Tech. J. 52, 843-886 (1973).

13. S. D. Personick, "Receiver Design for Optical Fiber Systems," Proc. IEEE 65, 1670-1678 (1977).

14. D. L. Snyder, Random Point Processes (Wiley, New York, 1975) Chap. 5.

15. H. L. Van Trees, Detection, Estimation and Modulation Theory, Part I (Wiley, New York, 1968), Chap. 4.

16. H. L. Van Trees, Detection, Estimation and Modulation Theory, Part I (Wiley, New York, 1968), Chap. 2.

17. R. M. Gagliardi and S. Karp, Optical Communications (Wiley, New York, 1976), Chap. 7.

18. D. L. Snyder, Random Point Processes (Wiley, New York, 1975), Chap. 6.

19. R. L. Mitchell, "Permanence of the Lognormal Distribution," J. Opt. Soc. Am. 58, 1267-1272 (1968).

20. B. K. Levitt, "Detector Statistics for Optical Communication through the Turbulent Atmosphere," Quart. Prog. Rept. 99, Research Lab. Electron., M.I.T., 114-123 (October 1970).

21. R. M. Gagliardi and S. Karp, Optical Communications (Wiley, New York, 1976), Chaps. 2, 3.

22. J. W. Goodman, "Some Effects of Target-Induced Scintillation on Optical Radar Performance," Proc. IEEE 53, 1688-1700 (1965).

23. L. Mandel, "Fluctuations of Photon Beams: the Distribution of Photo-electrons," Proc. Phys. Soc. 74, 233-242 (1959).

24. J. H. Shapiro, "Normal-mode Approach to Wave Propagation in the Turbulent Atmosphere," Appl. Opt. 13, 2614-2619 (1974).

25. C. W. Helstrom, Quantum Detection and Estimation Theory (Academic Press, New York, 1976), pp. 216-217.

26. D. L. Fried and R. A. Schmeltzer, "The Effect of Atmospheric Scintillation on an Optical Data Channel-Laser Radar and Binary Communications," Appl. Opt. 6, 1729-1737 (October 1967).

UNCLASSIFIED

SECURITY CLASSIFICATION OF THIS PAGE *(When Data Entered)*

| REPORT DOCUMENTATION PAGE | | READ INSTRUCTIONS BEFORE COMPLETING FORM |
|---|---|---|
| 1. REPORT NUMBER<br>ESD-TR-78-290 | 2. GOVT ACCESSION NO. | 3. RECIPIENT'S CATALOG NUMBER |
| 4. TITLE *(and Subtitle)*<br>Target Detection with a Direct-Reception Optical Radar | | 5. TYPE OF REPORT & PERIOD COVERED<br>Project Report |
| | | 6. PERFORMING ORG. REPORT NUMBER<br>Project Report TST-27 |
| 7. AUTHOR(s)<br>Jeffrey H. Shapiro | | 8. CONTRACT OR GRANT NUMBER(s)<br>F19628-78-C-0002 |
| 9. PERFORMING ORGANIZATION NAME AND ADDRESS<br>Lincoln Laboratory, M.I.T.<br>P.O. Box 73<br>Lexington, MA 02173 | | 10. PROGRAM ELEMENT, PROJECT, TASK AREA & WORK UNIT NUMBERS<br>Program Element No. 65705F<br>Project No. 649L |
| 11. CONTROLLING OFFICE NAME AND ADDRESS<br>Air Force Systems Command, USAF<br>Andrews AFB<br>Washington, DC 20331 | | 12. REPORT DATE<br>16 Nov 1978<br>13. NUMBER OF PAGES<br>66 |
| 14. MONITORING AGENCY NAME & ADDRESS *(if different from Controlling Office)*<br>Electronic Systems Division<br>Hanscom AFB<br>Bedford, MA 01731 | | 15. SECURITY CLASS. *(of this report)*<br>Unclassified<br>15a. DECLASSIFICATION DOWNGRADING SCHEDULE |

16. DISTRIBUTION STATEMENT *(of this Report)*

Approved for public release; distribution unlimited.

ESD-TR-78-290

17. DISTRIBUTION STATEMENT *(of the abstract entered in Block 20, if different from Report)*

TST-27

18. SUPPLEMENTARY NOTES

None

19. KEY WORDS *(Continue on reverse side if necessary and identify by block number)*

| | | |
|---|---|---|
| optical radar | target speckle | signal-to-noise ratio |
| direct reception | glint | optimum likelihood-ratio processor |
| atmospheric turbulence | atmospheric scintillation | single-pulse target detection |

20. ABSTRACT *(Continue on reverse side if necessary and identify by block number)*

A theoretical study of the use of a direct reception Nd:YAG laser radar for target detection is reported. This work builds from a mathematical system model which incorporates the statistical effects of propagation through atmospheric turbulence, target speckle and glint, and receiver noise; both photomultiplier and avalanche photodiode receivers are considered. Results are presented for the receiver signal-to-noise ratio which show, explicitly, the deleterious effects of atmospheric scintillation on system performance. The structure and performance of the optimum likelihood-ratio processor for single-pulse target detection are analyzed.

207 650 RLH

DD FORM 1 JAN 73 1473 EDITION OF 1 NOV 65 IS OBSOLETE

UNCLASSIFIED

SECURITY CLASSIFICATION OF THIS PAGE *(When Data Entered)*